

---

Theses and Dissertations

---

Spring 2014

## Stoker boiler CFD modeling improvements through alternative heat exchanger modeling

Albert J. Depman III  
*University of Iowa*

Follow this and additional works at: <https://ir.uiowa.edu/etd>



Part of the [Mechanical Engineering Commons](#)

Copyright 2014 Albert Depman

This thesis is available at Iowa Research Online: <https://ir.uiowa.edu/etd/4609>

---

### Recommended Citation

Depman, Albert J. III. "Stoker boiler CFD modeling improvements through alternative heat exchanger modeling." MS (Master of Science) thesis, University of Iowa, 2014.  
<https://doi.org/10.17077/etd.cwov9wir>

---

Follow this and additional works at: <https://ir.uiowa.edu/etd>



Part of the [Mechanical Engineering Commons](#)

STOKER BOILER CFD MODELING IMPROVEMENTS THROUGH ALTERNATIVE  
HEAT EXCHANGER MODELING

by  
Albert J. Depman III

A thesis submitted in partial fulfillment  
of the requirements for the Master of  
Science degree in Mechanical Engineering  
in the Graduate College of  
The University of Iowa

May 2014

Thesis Supervisor: Associate Professor Albert Ratner

Copyright by  
ALBERT J. DEPMAN III  
2014  
All Rights Reserved

Graduate College  
The University of Iowa  
Iowa City, Iowa

CERTIFICATE OF APPROVAL

---

MASTER'S THESIS

---

This is to certify that the Master's thesis of

Albert J. Depman III

has been approved by the Examining Committee  
for the thesis requirement for the Master of Science  
degree in Mechanical Engineering at the May 2014 graduation.

Thesis Committee: \_\_\_\_\_  
Albert Ratner, Thesis Supervisor

\_\_\_\_\_  
H. S. Udaykumar

\_\_\_\_\_  
Ching-Long Lin

To my family and friends

## ACKNOWLEDGMENTS

This thesis would not have been possible without the help and support of several individuals. First and foremost, I would like to extend my gratitude to my colleague and friend, Mohsen Ghamari, who lent his experience, opinions, and critiques numerous times throughout the research and composition of this work. My predecessor Xinhui Zhang's work in this area was very informative and an invaluable point of reference during the writing of this thesis. I am extremely thankful for my advisor, Professor Albert Ratner, who gave me guidance, direction, and motivation whenever I needed it.

Finally, my parents, Al and Barb Depman, have always given me nothing but unconditional love and support as I pursue and achieve my goals, and I am forever grateful to them.

## ABSTRACT

Accurate models and realistic simulations are essential in developing cleaner and more efficient coal- and biomass-fired boilers. Using the CFD simulation software Fluent The University of Iowa created a model of an industrial boiler that adequately compares the practice of co-firing biomass and coal against firing only coal. The simulations used in this comparison, show significant circulation zones and an unrealistic temperature profile inside the boiler heat exchanger region. This model is effective for comparing the relative decrease in emissions when co-firing with biomass versus exclusively coal combustion, but it does not present a realistic simulation of biomass or coal combustion.

The purpose of the current work is to develop a more realistic baseline coal combustion model. Calculations for the proximate and ultimate analysis of coal, as well as properties necessary for energy and mass flux computations, have been updated in the current model. The fuel bed model – a simple two-dimensional distribution of energy and mass fluxes from the grate – was kept the same due to the complexities of fuel bed modeling. Simulation boundary conditions and flow models were tested and modified to determine the most realistic model settings. The geometry and mesh grid of the boiler model were also varied in an attempt to fix problematic areas.

Several approaches were implemented in an effort to reduce the circulation zones and generate a realistic temperature profile. The negative energy source term in the boiler representing the energy removed by the water pipes in the heat exchanger was analyzed, and different configurations of this sink were tested. Finally, the heat exchanger models built in to Fluent were studied and implemented. These models proved to be the most effective in reducing recirculation zones and decreasing high temperature gradients. While the current model of the coal-fired boiler has a higher overall temperature than the previous one, circulation zones are almost completely eliminated, the flow path has been improved, and the temperature profile in the boiler is more realistic.

## TABLE OF CONTENTS

LIST OF TABLES .....	vi
LIST OF FIGURES .....	vii
CHAPTER 1: INTRODUCTIONS.....	1
1.1 Motivations.....	1
1.2 Objectives .....	2
1.3 Organization .....	3
CHAPTER 2: LITERATURE REVIEW .....	4
2.1 Fuel Bed Modeling .....	4
2.2 CFD Modeling.....	8
2.3 Coal Combustion Chemistry.....	11
2.4 Turbulent Models.....	15
2.4.1 $k - \varepsilon$ Models.....	16
CHAPTER 3: PREVIOUS UNIT 10 BOILER CFD MODEL.....	20
3.1 Geometry and Mesh Grid .....	21
3.2 Coal Analysis.....	24
3.3 Coal Bed Model.....	24
3.4 Boundary Conditions.....	26
3.6 Flow Models and Heat Exchanger.....	27
3.7 Previous Unit 10 Simulation Results.....	28
CHAPTER 4: CURRENT UNIT 10 BOILER MODEL .....	32
4.1 Coal Analysis.....	32
4.1.1 Coal Properties .....	32
4.1.2 Bed Model .....	33
4.2 Boundary Conditions and Flow Models.....	34
4.2.1 Turbulence Model .....	35
4.2.2 Radiation Model .....	41
4.2.3 Inlet Velocities.....	43
4.3 Geometry and Mesh Grid .....	46
4.3.1 Mesh .....	48
4.3.2 Geometry .....	51
4.4 Heat Exchanger Modifications .....	56
4.4.1 Energy Source Terms .....	56
4.4.2 Fluent Heat Exchanger Model.....	61
CHAPTER 5: CONCLUSIONS .....	82
5.1 Conclusions.....	82
5.2 Future Work.....	84
REFERENCES .....	85



## LIST OF TABLES

Table 2.1. Proximate analysis of Eastern Bituminous coal .....	12
Table 2.2. Ultimate analysis of Eastern Bituminous coal.....	12
Table 3.1. Coal analyses used in previous Unit 10 simulations.....	24
Table 3.2. Air inlet boundary conditions for previous Unit 10 simulations .....	26
Table 3.3. Temperature boundary conditions for previous Unit 10 simulations .....	27
Table 4.1. Proximate analyses of coal used in current Unit 10 simulations.....	32
Table 4.2. Ultimate analyses of coal used in current Unit 10 simulations.....	33
Table 4.3. Wall temperatures of selected areas in the model.....	35
Table 4.4. Air inlet boundary conditions .....	35
Table 4.5. Mesh sizing techniques, their performance and number of element nodes.....	48
Table 4.6. Various heat exchanger model parameter and settings.....	66
Table 4.7. Comparison of final convergence values for key equations .....	81

## LIST OF FIGURES

Figure 3.1. Previous Unit 10 geometry sectioning .....	21
Figure 3.2. Isometric view of previous boiler geometry.....	22
Figure 3.3. Previous Unit 10 boiler mesh grid.....	23
Figure 3.4. Grate heat flux distribution.....	25
Figure 3.5. Temperature profile in the boiler.....	29
Figure 3.6. O <sub>2</sub> concentration profile .....	29
Figure 3.7. CO <sub>2</sub> concentration profile.....	30
Figure 4.1. Flow chart for the simulations discussed in Section 4.2 .....	34
Figure 4.2. Temperature profile for initial simulation of current model .....	36
Figure 4.3. Velocity vector profile for initial simulation of current model .....	37
Figure 4.4. Temperature profile using RNG turbulence model .....	38
Figure 4.5. Velocity vector profile using RNG turbulence model.....	39
Figure 4.6. Temperature profile using standard turbulence model.....	40
Figure 4.7. Velocity vector profile using standard turbulence model.....	41
Figure 4.8. Temperature profile using discrete ordinates radiation model.....	43
Figure 4.9. Temperature profile for 15 m/s small inlet velocity boundary condition.....	44
Figure 4.10. Temperature profile for 10 m/s small inlet velocity boundary condition.....	45
Figure 4.11. Flow chart for the simulations discussed in Section 4.3 .....	46
Figure 4.12. Modified geometry used in current Unit 10 simulations.....	47
Figure 4.13. Temperature profile using a refined grate mesh grid .....	49
Figure 4.14. Comparison of the temperature profile between models with a refined heat exchanger mesh grid (left) and without (right) .....	50
Figure 4.15. Comparison reduced geometry (left) and original geometry (right) .....	52
Figure 4.16. Temperature profile using reduced geometry.....	52
Figure 4.17. Velocity vector profile using reduced geometry .....	53
Figure 4.18. Boiler model with slotted slope geometry.....	54

Figure 4.19. Temperature profile using slotted slope geometry .....	55
Figure 4.20. Flow chart for the simulations discussed in Section 4.4 .....	56
Figure 4.21. Temperature profile with the stack volume containing 33% of the negative energy source term .....	58
Figure 4.22. Temperature profile with the stack volume containing 50% of the negative energy source term .....	59
Figure 4.23. Modified heat exchanger volume geometry .....	60
Figure 4.24. Temperature profile using modified heat exchanger volume geometry.....	61
Figure 4.25. Macro sectioning used in Fluent heat exchanger models.....	62
Figure 4.26. Temperature profile from initial Fluent heat exchanger model simulation.....	68
Figure 4.27. Velocity vector profile from initial Fluent heat exchanger model simulation.....	69
Figure 4.28. Temperature profile using simple effectiveness model.....	70
Figure 4.29. Temperature profile using Fixed Heat Rejection .....	71
Figure 4.30. Temperature profile using NTU model with three passes.....	73
Figure 4.31. Temperature profile using NTU model with four passes .....	73
Figure 4.32. Temperature profile using NTU model with five passes.....	74
Figure 4.33. Temperature profile using NTU model with six passes .....	74
Figure 4.34. Velocity vector profile using NTU model with three passes .....	75
Figure 4.35. Velocity vector profile using NTU model with four passes.....	75
Figure 4.36. Velocity vector profile using NTU model with five passes .....	76
Figure 4.37. Velocity vector profile using NTU model with six passes.....	76
Figure 4.38. Temperature profile using NTU model with five passes and six rows .....	77
Figure 4.39. Temperature profile using NTU model with five passes and 10 rows.....	78
Figure 4.40. Temperature profile using NTU model with five passes and 15 rows.....	78
Figure 4.41. Temperature profile using NTU model with 6 rows in combination with 10 m/s small secondary inlet velocity.....	79
Figure 4.42. Temperature profile using NTU model with 10 rows in combination with 10 m/s small secondary inlet velocity.....	80

## CHAPTER 1: INTRODUCTIONS

### 1.1 Motivations

As the developed world transitions toward renewable power sources such as wind energy, biomass combustion and nuclear fusion, the need grows for fast, reliable and accurate modeling techniques that can be used to assess the efficiency and performance of these sources before they are physically implemented. These models and simulations also allow companies to determine the cost-effectiveness and environmental impact of adding renewable fuels to standard fossil fuels such as coal or gasoline, or using renewable resources to replace fossil fuels altogether. For instance, some power plants use numerical modeling and Computational Fluid Dynamics (CFD) simulations to predict the reduction in emissions when co-firing biomass with pulverized coal.

The first steps in this process are to develop a model that accurately represents an existing system and then using that model to make further predictions. In the case of coal, past research has focused mainly on numerical modeling techniques, which can be slow and computationally expensive. For this reason, CFD modeling strategies are useful for the visualizations and quick predictions necessary to evaluate different fuel options and combinations.

Due to their simple design and ability to burn many different types of fuels, stoker boilers are the most common power producing systems used for the evaluation of renewable fuels, including natural gas and various biomasses. They were initially designed to burn pure coal, however, so CFD simulations and models must begin analyses by using multi-scale techniques to create baseline coal simulations and predictions. In their most general form, these multi-scale techniques consist of the modeling of solid combustion, gas fluid flow and particle movement (including turbulence), and gaseous combustion.

## 1.2 Objectives

Recognizing the need for a reliable and accurate baseline coal combustion model for a stoker boiler, this work details the techniques used in creating working simulations, and describes and attempts to explain various issues encountered during the modeling process. The primary goal of this research is to develop a realistic CFD model for the burning of pure coal based off previous modeling work, which can then be used in the future for things such as investigating the effect of co-firing natural gas or biomass with coal, predicting emission levels from pure coal combustion and from various combinations of coal and renewable fuels, and determining the effect of different coal loading conditions on other similar stoker boilers.

Two objectives result from this primary goal. The first is to determine boundary conditions and flow behaviors for use in the CFD simulation, which include, but are not limited to, turbulent flow models, radiation models, energy sources, air velocities and wall temperatures. Using the commercial software ANSYS Fluent, these boundary conditions and flow models will be varied and tested to determine the combinations resulting in the most realistic temperature profiles and flow paths.

The second objective is to research, implement, and test the heat exchanger models built in to the Fluent software. Results from previous simulations on the same stoker boiler showed problematic regions in the heat exchanger area of the boiler model. The major issues included very large temperature gradients, unrealistic temperature magnitudes, and intense flow circulation zones. The Fluent heat exchanger models, along with the boundary conditions and flow models tested earlier in the work, will be used to attempt to reduce these temperature gradients and circulation regions, while keeping a realistic temperature profile and flow path in the boiler.

### 1.3 Organization

Motivations and objectives for the work and the arrangement of this thesis are found in Chapter 1. Chapter 2 presents a brief literature review of boiler modeling, split into two major sections: fuel bed modeling and CFD simulation techniques. It also covers basic coal combustion theory and turbulent model theory. Previous modeling of the specific boiler studied in this work is covered in Chapter 3, highlighting the fuel bed modeling, boundary conditions and flow models used in the CFD simulations, and the results are discussed. Chapter 4 details modifications made to the previous model and outlines various simulations and tests utilized in the attempt to achieve a realistic temperature profile and flow path within the boiler. It also includes the theory and implementation of heat exchanger models built in to the Fluent software. The thesis concludes in Chapter 5 by discussing significant results and how well the objectives were achieved in the work. Future modeling considerations and possibilities are outlined as well and areas of improvement are noted.

## CHAPTER 2: LITERATURE REVIEW

### 2.1 Fuel Bed Modeling

The Unit 10 stoker boiler at the University of Iowa (UI) power plant uses a moving grate on to which pulverized coal is thrown. The modeling of the combustion of the coal on this moving grate is very complex and effort has been made in the past to come up with simplified models for use in CFD. The most common are fixed-bed models, utilizing either transient combustion calculations or approximate reaction equations in order to determine the boundary conditions at the grate resulting from the combustion of the solid fuel on the bed. Due to the popularity of fixed-bed modeling, there are multiple approaches for it found in the literature: one-dimensional in space, one-dimensional in time, two-dimensional in space, and models that combine spatial and transient analyses. Fully three-dimensional models can be developed and solved using methods such as Direct Numerical Simulation, but these are very computationally expensive.

The simplest model for fixed bed modeling is a one-dimensional model of the heat release and concentration profiles over the grate length. Goerner and Klasen used this approach to approximate the temperature profile over the grate by integrating the heat generation profile over the grate, which was determined with mathematical submodels created by the Institutes of Environmental Process Engineering and Plant Design, and by solving basic equations for the relation between temperature and sensible and latent heat release. They also determined concentration profiles for the species involved in the combustion by using simple balanced reaction equations. In validating their results, the researchers found that while the trends of the measured temperatures and the modeled ones were fairly similar, there was significant error in the magnitude of the temperatures. According to the authors, this error most likely resulted from the simplified

reaction equations, which did not include non-stationary process conditions (Goerner 2006).

A one-dimensional transient model for a fixed bed was developed by Zhou et al. in order to perform numerical simulations of straw combustion (Zhou 2005). The model is transient only for the reaction calculations for the solid phase combustion, so it was not able to be used to approximate a moving grate. Since it utilized transient combustion, the solid phase and gas phase reactions were coupled into a four step process: evaporation of moisture, volatile release/char formation, burning of the volatiles, and the oxidation of the char particles. According to the researchers in the paper's conclusion, results from the simulation of the numerical model were reasonably consistent with the experimental data obtained.

A two-dimensional mathematical model was developed by van der Lans et al. to predict straw combustion on a moving bed (van der Lans 2000). The model included the horizontal position of the straw along the grate as well as the vertical position, so it could be used to roughly approximate a moving grate using steady state calculations instead of needing to solve complex partial differential equations with transient terms. The researchers assumed that the  $O_2$  from the air only reacted with the carbon left on the grate after devolatilization of the straw, thereby decoupling the solid phase and gas phase reactions. This is a large simplification, but the bed temperature results from their simulations matched up fairly well to their experimental data.

Wei et al. also utilized a two dimensional approach in simulating a biomass waste boiler with an inclined moving grate and a coal boiler with a horizontal moving grate (Wei 2001). For both cases, the researchers reduced the complexity of the bed combustion by splitting the grate up into well-defined zones and decoupling the gas phase reaction from the solid phase reaction occurring on the bed. The boundary conditions at the grate bed were then determined using the mass and energy balances of the solid fuel combustion. Defining zones on the grate in this way makes it possible to



simulate the moving grate by assuming steady state and a fixed bed, giving a fuel distribution along the bed horizontally and vertically.

Another transient combustion model was developed by Ford et al. The researchers discretized the fuel bed into a series of boxes, not unlike the zoning carried out by Wei et al. Coal enters as uniform size spherical lumps stacked atop one another. As the fuel moves along the grate, the size of the box containing the coal may decrease depending on how much of the coal was burned during the 1-minute long reactions inside each box along the grate (Ford 1993). In this model, like most of the other ones, the solid combustion is separate from the volatile combustion above the grate. However, the transient nature of the model makes for a good approximation of the moving grate in a real boiler, and the results of the simulation for the fuel bed temperature along the grate and the amount of carbon released from the coal are consistent with measured data.

Kaer et al. used Lagrangian tracking and the one-dimensional heat conduction model in their simulation of a biomass fuel bed (Kaer 2005). This approach differs from the previously discussed models because it follows particles of the fuel in time, instead of observing the reactions of the fuel at specified points in space along the bed. By solving the mass and energy conservation equations and using the one-dimensional (in time) heat conduction equation, the researchers were able to determine the transient combustion of the fuel particle through drying, devolatilization and char oxidation. The results of the model for mass flux and air temperature were consistent with the trends observed in measurements.

For the mathematical modeling of straw combustion in a power plant furnace, Yang et al. created a unique mathematic model to simulate burning on a moving grate. Similar to Kaer, the research team utilized a Lagrangian approach. Eight major assumptions were made for the model, some of which include: the bed was considered a porous medium, combustion occurs layer by layer with ignition starting from the top of the bed, the bed is moved forward at a constant speed, and the fuel was represented by

spherical particles with an equivalent diameter, which were then distributed uniformly in the width direction of the bed so that the solution only requires two dimensions (Yang 2007). The grate vibration causes particle mixing, which was simulated using diffusion theory. An approximate diffusion coefficient was determined by visually observing that the combustion on the bed completes at 2/3 of the grate's length. Modified continuity, energy and species transport equations were used for the calculations, with bed speed taken into account by a constant parameter. The equations were discretized and solved in time and space using code developed by the authors (FLIC code) and a discretization method proposed by Pantankar (Pantankar 1980). The predicted temperature and CO concentrations from this straw combustion grate model were compared to measurement data used in the work of van der Lans et al. (discussed previously in this section) and the results were found to be in very good agreement. Some uncertainty arose from locating the exact measurement locations from the van der Lans data, but the Yang simulation followed the trends very accurately. The research team concluded that the mathematical methods employed were reliable for analysis of straw combustion in a packed-bed furnace (Yang 2007).

By examining these examples of common fixed-bed modeling techniques, some broad similarities can be observed. Most of the methods decouple the solid-phase and gas-phase reactions in order to simplify the model, but still end up with reasonably accurate simulation results when compared to the measured data. The main method of discretization is an Eulerian approach: observing a certain location in space on the fixed grate and calculating the reactions of the fuel within that space, though two papers (Kaer and Yang) showed that a Lagrangian approach is also effective. The most important goal of fixed-bed modeling is to determine the boundary conditions present in the grate region after the solid combustion on the fuel bed, in order to effectively and accurately simulate the gas phase reaction above the grate.

## 2.2 CFD Modeling

After the fuel bed is sufficiently modeled, the gas-phase reactions and turbulent mixing present in the furnace above the grate and in the heat exchanger portion of the boiler need to be approximated. The first two stages, fuel bed combustion and the burning in the furnace, are commonly decoupled in order to reduce the complexity of the reaction chemistry and to be able to use CFD software to model the high temperature combustion and turbulent flows. Heat exchanger modeling methods varied between more complex convective heat exchanger models and simple energy source term representations.

For the simulation of fixed bed biomass boilers, Sharler et al. used the CFD software ANSYS Fluent to model the turbulent reactive flow above the grate after using their own developed model for the fixed bed combustion. The researchers chose the realizable  $k - \varepsilon$  model to simulate turbulent mixing, the discrete ordinates model for the radiation, and the eddy dissipation model, in conjunction with a 3-step reaction of the biomass volatiles, for the gas-phase combustion (Sharler 2004). The primary goal of the research team was to introduce their own convective heat exchanger model, which takes into account the influence of flow direction and patterns on the various tube banks of the heat exchanger: the evaporator, superheater and economizer. Results showed that CFD simulation values for the temperature in the furnace matched very well to measured temperatures at various points inside the furnace.

Lin et al. modeled a tangentially-fired coal boiler using slightly different modeling techniques, necessitated by the fact that there is no fixed bed and the pulverized coal is injected with the primary air source from the corners of the furnace. The calculation domain was meshed with a structured grid using a first-order spatial scheme. This discretization allowed grid-independent solutions while limiting the error as much as possible and keeping computation time relatively low. The coal particle streams were tracked using a Lagrangian method, and the chemical reactions included the particle

devolatilization and char combustion, culminating in the use of a probability density function for the gas-phase reactions. The standard  $k - \varepsilon$  model was used to solve for the Reynolds equations representing the turbulent flow and mixing, and flow field prediction was done using the SIMPLE method. Radiation was modeled using the discrete ordinates model because it is able to account for particulate effects and localized heat sources, both of which are present when simulating particle stream combustion. In the particular paper cited, the heat exchanger is approximated using porous panels at a certain specified temperature, using only radiation heat transfer in the energy conservation calculations. The researchers mentioned that they added convective heat transfer to the heat exchanger model in separate simulations but that it did not contribute significantly to the gas temperature deviation in the boiler (Lin 2003).

As previously discussed, the research group of Yang et al. created their own unique code to simulate a bed model for a straw-based power plant furnace (Yang 2007). Using the Fluent software, this bed model was integrated with a CFD model for the over-bed combustion. The turbulent flow in the furnace region was represented using the two-equation standard  $k - \varepsilon$  model, and the discrete-ordinates model was used to model the radiation heat transfer. Fluent calculated the radiation absorption coefficient based on the characteristic cell-size of the mesh elements and the gas concentrations in the furnace. In order to simulate the out-of-bed volatile combustion, the eddy-breakup/finite rate model was selected. The eddy-breakup model was chosen because the turbulence of the flow in the boiler results in the reaction rate being controlled by the mixing of the reactants, which is an assumption that the model makes. In order to simplify the gas-phase reactions, it was assumed that the reaction rate was only temperature dependent, leading to the selection of the finite rate model to go along with the eddy-breakup model. The fuel bed model computation resulted in values for temperature, velocity, mass flux and concentration values for the species involved in the combustion. These fluxes and parameters were given to Fluent as boundary conditions for the bed combustion, and

Fluent's simulation of the over-bed combustion produced some radiation flux and temperature variation, which was also incident on the fuel bed. Because of the intrinsic nature of this relationship, the two simulations were iterated to some convergence criterion. The heat exchanger portion of the boiler was modeled in a very basic way with the superheaters being represented as plates of a specified temperature, taking energy from the flow by radiation heat transfer alone. The researchers primarily compared species concentrations, temperature profiles and combustion efficiency with measured data and deemed the agreement between model results and plant operation satisfactory (Yang 2007).

Miltner et al. developed a CFD process for the simulation of a biomass-fired combustion chamber in order to predict emissions such as carbon monoxide and nitrogen oxide (Miltner 2007). The researchers used the CFD solver Fluent to calculate the stationary flow after discretizing the geometry into approximately 1.5 million volumetric cells. To model the turbulent effects in the combustion zone, an SST- $k-\omega$  turbulence model was used because of its applicability to free jets and swirling free jets. For radiation heat transfer calculations, the DTRM model was used because of its small computational expense and ability to handle fairly opaque media. In order to balance mass and energy, volume sinks and sources were created inside the boiler. The assumption implicit in this strategy is that the gas phase combustion was infinitely fast, meaning that as soon as the reactants mixed together due to the turbulence they were already burned. This assumption lowers the computational time significantly. When comparing the measured and simulated temperatures and volume flows in the boiler, the researchers found that their model was rather accurate, with much of the error coming from the fact that they modeled the boiler walls as adiabatic (insulated), when in reality heat will escape from the furnace through the walls. The species concentration results were not nearly as accurate as the temperature predictions, most likely because the combustion models for the solid and gas phase reactions were very simplified.

Even from the small sample of research presented above, it is clear that the most popular CFD software used in combustion modeling is the ANSYS-made Fluent solver. It contains many turbulent flow and radiation models and excels at turbulent mixing and heat transfer computations. Fluent also has a large database of species models and is able to simulate many reactions, including combustion, very accurately and efficiently. For more advanced combustion and species interactions, Fluent even has various injection models, which can be used to model fuel sprays or tangentially-fired fuel particles interacting with other fluid flows. All of these aspects allow Fluent to be a popular choice for the modeling and simulation of industrial sized boilers, and this is evident from the cases presented in earlier sections.

Within the Fluent software, the most common models used by researchers were the  $k - \varepsilon$  models for turbulent flow and mixing, the discrete ordinates model for radiation, and eddy dissipation models for the reaction kinetics. When balancing the energy during combustion, the simplest methods were used most often, with energy sources and sinks or constant temperature plates being utilized to simulate heat transfer by radiation, though some methods still include some convection heat transfer effects.

### 2.3 Coal Combustion Chemistry

Many of the previously discussed boiler or combustion models deal primarily with biomass combustion or the effects of coal being co-fired with different biomasses. This information is good for determining the best methods to model turbulent mixing and combustion reaction kinetics in a boiler, but the actual species and reaction steps of coal combustion need to be considered further if a working model of a coal-fired boiler is to be developed.

Coal can be grouped into two main categories: bituminous and subbituminous coal. The largest group is bituminous coals, and they are characterized as having a lower

amount of fixed carbon matter and a relatively high volatile and sulfur content. Heating values for bituminous coals range from 24.4 to 32.6 MJ/kg. Subbituminous coals have higher moisture content than bituminous coals, as well as lower sulfur content and a higher amount of volatile matter. These coals have heating values in the range of 19.3 to 26.7 MJ/kg (Babcock 1975). The chemical and physical properties of Eastern Bituminous coal, including the ultimate and proximate analyses, are shown in Tables 2.1 and 2.2.

Table 2.1. Proximate analysis of Eastern Bituminous coal

	Proximate Analysis [wt %]
Moisture	5.85
Volatile Matter	35.61
Fixed Carbon	47.94
Ash	10.6
Total	100
HHV [MJ/kg]	28.47
Density [kg/m <sup>3</sup> ]	1346

Table 2.2. Ultimate analysis of Eastern Bituminous coal

	Ultimate Analysis [wt %]
Moisture	5.85
Carbon	68.16
Hydrogen	4.77
Nitrogen	1.54
Oxygen	7.78
Sulfur	1.3
Ash	10.6
Total	100

In a coal-fired boiler, the coal starts a devolatilization process as soon as it is thrown onto the high-temperature fuel bed region, and continues as the carbon on the bed is burned. The gases released during devolatilization burn during the secondary reaction, which takes place in the gaseous combustion zone above the grate where secondary air streams enter the boiler. A general model for coal devolatilization is presented by Solomon et al. as follows: Bituminous coal undergoes primary pyrolysis by decomposing into functional groups, releasing CO<sub>2</sub>, some CH<sub>4</sub> and H<sub>2</sub>O, and light aliphatic gases (molecules that do not contain benzene or aromatic rings). The coal then begins secondary pyrolysis, wherein it releases HCN, H<sub>2</sub> and CO, and additional methane evolution occurs (Solomon 1988).

Products of bituminous coal combustion, including bed and gaseous reactions, have been determined by the United States Environmental Protection Agency. The products fall into several categories: particulate matter, sulfur oxides, nitrogen oxides, carbon monoxide, organic compounds, trace metals, acid gases, fugitive emissions, and greenhouse gases. Nearly 99 percent of the bed combustion (burning of solid carbon chunks) is converted into CO<sub>2</sub>, so most of the emission products are a result of the gaseous combustion above the grate.

The particulate matter in coal combustion products consists of coal ash, settled out in the boiler as bottom ash or entrained in the flue gas as fly ash. This soot needs to be blown off heat transfer surfaces periodically, as well as away from the air preheater, economizer and convective sections of the boiler.

Sulfur oxide emissions contain mostly SO<sub>2</sub>, with trace amounts of SO<sub>3</sub> and other gaseous sulfates. Of the sulfur present in the coal, about 95 percent will be released as SO<sub>x</sub>. Nitrogen oxide emissions are primarily NO, with small amounts of NO<sub>2</sub> and N<sub>2</sub>O. On average, only 20-60 percent of the nitrogen in the fuel is converted to NO<sub>x</sub>, and the concentration is found to be highly dependent on temperature, with higher concentrations



resulting from lower combustion temperatures. Gas residence time and the amount of nitrogen in the flame are also correlated to the amount of  $\text{NO}_x$  released.

The amount of CO emissions from the coal combustion is dependent on the fuel oxidation efficiency, which can be maximized by using a properly operated and maintained boiler. Combustion in a large boiler generally results in a lower amount of CO than a smaller boiler because there is a longer gas residence time, so complete combustion can often be achieved.

In the same manner as with CO emissions, a boiler with high combustion efficiency will have a lower rate of organic compound release. The organic compounds that do get emitted consist of alkanes, alkenes, alcohols, benzenes, and other unburned vapor-phase hydrocarbons. It follows that the main cause of organic emissions is incomplete combustion in the gaseous region.

Both trace metal emissions and acid gas emissions can be absorbed into the fly or bottom ash. Of the matter that isn't absorbed, particulate matter controls can capture the trace metals, and the most common acid gases (HCN and HF) can be controlled easily by scrubbing systems as they are water soluble. Fugitive emissions are simply pollutants that escape during transfer, storage or materials handling, and can also come from leakage in the industrial process. The primary emission of this type is particulates, usually fly ash that is not caught by the filters or venting used to handle it.

Greenhouse gas emissions during coal combustion primarily consist of  $\text{CO}_2$ , with smaller amounts of  $\text{CH}_4$  and  $\text{N}_2\text{O}$ . The  $\text{CO}_2$  emissions can be somewhat controlled and reduced by the formation of CO, but the amount of CO emitted during combustion is insignificant compared to the  $\text{CO}_2$ . Since most of the  $\text{CO}_2$  comes from the solid carbon combustion on the bed, the amount emitted depends highly on the carbon content of the specific coal used in the boiler. As discussed above,  $\text{N}_2\text{O}$  formation depends on the fuel oxidation efficiency and operation and maintenance of the boiler.  $\text{CH}_4$  emissions generally occur with conditions that also favor  $\text{N}_2\text{O}$  formation.

Out of all the coal combustion products,  $\text{NO}_x$  is a large concern to the EPA because the  $\text{N}_2\text{O}$  present in these emissions contributes to the depletion of the ozone layer and can also cause smog and acid rain. Some controls used in coal-fired boilers to suppress  $\text{NO}_x$  formation during combustion are low excess air, overfire air, and reburn. Having a low amount of excess air in the burner region means that there is less oxygen in the gaseous combustion region, leading to the inhibition of  $\text{NO}_x$  formation. The overfire air control consists of diverting some of the air used in combustion to ports above the main combustion zone. This process delays the combustion and lowers the overall reaction flame temperature, thereby reducing  $\text{NO}_x$  formation. Overfire air also mitigates the evolution of volatile fuel nitrogen by reducing the concentration of air in the main combustion zone. A lower amount of volatile nitrogen leads to a slower  $\text{NO}_x$  formation rate. Reburn means that a second combustion zone downstream is introduced, where additional fuel and air is injected and burned so that the  $\text{NO}_x$  produced in the first combustion region is converted to nitrogen and water. The additional air and fuel is then combusted completely by adding overfire air after this reburn region.

#### 2.4 Turbulent Models

The nature of high temperature and high speed combustion of the volatiles released from coal burning on the fuel bed is that of a highly turbulent and mixing flow. For this reason, the modeling of boilers and furnaces must include some type of turbulent modeling in order to represent this combustion and flow in a steady state manner. These models greatly reduce the complexity introduced by the turbulent mixing.

To simplify the governing equations (continuity, momentum and energy), Reynolds-Averaged Navier-Stokes (RANS) equations are most commonly used. RANS equations apply time averaging to filter out all turbulent eddies using a Reynolds stress

tensor. Time averaging is an assumption made to represent all properties varying continuously in time with approximate steady state values. This process is done by using the Reynolds Decomposition, shown in Equation 1.

$$u(x, t) = \bar{u}(x) + u'(x, t) \quad (1)$$

The right side of Equation 1 represents the quantity being broken in to a time-averaged component ( $\bar{u}$ ) and a fluctuating component ( $u'$ ). Each instantaneous property in an equation is decomposed in this way and then the resulting equation is time averaged.

As an example, the RANS simplification of the differential momentum transport equation in tensor notation is given in Equation 2. RANS is also applied to the continuity and energy transport Navier-Stokes equations in order determine all aspects of the turbulent flow.

$$\bar{u}_j \frac{\partial \bar{u}_i}{\partial x_j} = f_i - \frac{1}{\rho} \frac{\partial \bar{p}_i}{\partial x_i} + \nu \frac{\partial^2 \bar{u}_i}{\partial x_j \partial x_j} - \frac{\partial \overline{u'_i u'_j}}{\partial x_j} \quad (2)$$

#### 2.4.1 $k - \varepsilon$ Models

Putting focus on the momentum transport equation,  $k - \varepsilon$  models make use of a Reynolds stress tensor to approximate ejection and sweep events associated with turbulent vertical structures. The Reynolds stress tensor is given in Equation 3, and the Boussinesq eddy-viscosity approximation, shown in Equation 4, is applied.

$$\tau_{ij} = -\rho \overline{u'_i u'_j} \quad (3)$$

$$-\rho \overline{u'_i u'_j} = \mu \left( \frac{\partial \overline{u}_i}{\partial x_j} + \frac{\partial \overline{u}_j}{\partial x_i} \right) + \frac{2}{3} \rho \delta_{ij} k \quad (4)$$

The solution of Equation 4 depends on the turbulence kinetic energy ( $k$ ), which in turn depends on the turbulence dissipation rate ( $\varepsilon$ ). Both of these properties can be solved for in transport equations created by Launder and Spalding in 1972. These transport equations, given below in Equations 5 and 6, comprise the standard  $k - \varepsilon$  model (Launder 1972).

$$\frac{\partial}{\partial t} (\rho k) + \frac{\partial}{\partial x_i} (\rho k u_i) = \frac{\partial}{\partial x_j} \left[ \left( \mu + \frac{\mu_t}{\sigma_k} \right) \frac{\partial k}{\partial x_j} \right] + G_k + G_b - \rho \varepsilon - Y_M + S_k \quad (5)$$

$$\frac{\partial}{\partial t} (\rho \varepsilon) + \frac{\partial}{\partial x_i} (\rho \varepsilon u_i) = \frac{\partial}{\partial x_j} \left[ \left( \mu + \frac{\mu_t}{\sigma_\varepsilon} \right) \frac{\partial \varepsilon}{\partial x_j} \right] + C_{1\varepsilon} \frac{\varepsilon}{k} (G_k + C_{3\varepsilon} G_b) - C_{2\varepsilon} \rho \frac{\varepsilon^2}{k} + S_\varepsilon \quad (6)$$

In these equations,  $G_k$  (generation of turbulence kinetic energy due to mean velocity gradients) and  $G_b$  (generation of turbulence kinetic energy due to buoyancy) are found using Equations 7 and 8, and  $\mu_t$  (the eddy viscosity) is calculated as a combination of  $k$  and  $\varepsilon$  in Equation 9.

$$G_k = -\rho \overline{u'_i u'_j} \frac{\partial u_j}{\partial x_i} \quad (7)$$

$$G_b = \beta g_i \frac{\mu_t}{Pr_t} \frac{\partial T}{\partial x_i} \quad (8)$$

$$\mu_t = \rho C_\mu \frac{k^2}{\varepsilon} \quad (9)$$

The model constants used in the standard  $k - \varepsilon$  equations are  $C_{1\varepsilon} = 1.44$ ,  $C_{2\varepsilon} = 1.92$ ,  $C_\mu = 0.09$ ,  $\sigma_k = 1.0$ , and  $\sigma_\varepsilon = 1.3$ . These constants are the default ones used in the ANSYS Fluent modeling software when the standard  $k - \varepsilon$  turbulence model is applied.

A common variation on the standard  $k - \varepsilon$  turbulence model is the realizable  $k - \varepsilon$  model. From the Fluent documentation:

“the term ‘realizable’ means that the model satisfies certain mathematical constraints on the normal stresses, consistent with the physics of turbulent flows”

The main change in this model is that the Reynolds stress and the eddy viscosity equations are combined to form a new one, Equation 10, which gives the normal Reynolds stress in an incompressible strained mean flow.

$$\overline{u^2} = \frac{2}{3}k - 2\nu_t \frac{\partial U}{\partial x} \quad (10)$$

The normal stress  $\overline{u^2}$  will become negative (“non-realizable”) when the strain in the flow satisfies the inequality given in Equation 11. Then the  $C_\mu$  term is plugged into the eddy viscosity equation (Equation 9), and  $\nu_t$  is found by dividing  $\mu_t$  by density. Therefore the realizable model is only valid when  $\overline{u^2}$  remains positive (“realizable”).

$$\frac{k}{\varepsilon} \frac{\partial U}{\partial x} > \frac{1}{3C_\mu} \approx 3.7 \quad (11)$$

The equation for  $k$  remains the same as in the standard model (Equation 5), but the equation for  $\varepsilon$  changes to Equation 12, shown below, with the main difference being that the term representing the production of  $\varepsilon$  no longer depends on  $k$ .

$$\frac{\partial}{\partial t}(\rho\varepsilon) + \frac{\partial}{\partial x_i}(\rho\varepsilon u_i) = \frac{\partial}{\partial x_j} \left[ \left( \mu + \frac{\mu_t}{\sigma_\varepsilon} \right) \frac{\partial \varepsilon}{\partial x_j} \right] + \rho C_{1\varepsilon} S_\varepsilon - \rho C_{2\varepsilon} \frac{\varepsilon^2}{k + \sqrt{\nu \varepsilon}} + C_{1\varepsilon} \frac{\varepsilon}{k} (C_{3\varepsilon} G_b) + S_\varepsilon \quad (12)$$

where

$$C_1 = \max \left[ 0.43, \frac{\eta}{\eta + 5} \right], \quad \eta = S \frac{k}{\varepsilon}, \quad S = \sqrt{2S_{ij}S_{ij}}$$

Another notable change present in the realizable version of the  $k - \varepsilon$  model is that the term  $C_\mu$  in the eddy viscosity equation is not constant as before, and varies according to Equation 13.

$$C_\mu = \frac{1}{A_0 + A_S \frac{kU^*}{\varepsilon}} \quad (13)$$

$U^*$  and other parameters can be found in the Fluent documentation but are not necessary at this time to describe the realizable model any further. Kim et al. and Shih et al. are two examples of research done to validate the realizable  $k - \varepsilon$  model for many flows, including channel and boundary layer flows, separated flows, free flows with jets and mixing layers, and rotating homogenous shear flows. The results of the validation show markedly better performance of the realizable model versus the standard one for these types of flow cases. The realizable model also predicts the spreading rate for axisymmetric jets as well as for planar jets (the so-called round-jet anomaly); something the standard model is not able to do (Kim 1997, Shih 1995).

### CHAPTER 3: PREVIOUS UNIT 10 BOILER CFD MODEL

The previous model of the Unit 10 stoker boiler used for simulations at the University of Iowa was done by Xinhui Zhang. The geometry is split into four main sections: the grate volumes, a large volume representing the furnace, a section for the heat exchanger pipes, and a volume for the stack outflow. Figure 3.1 below shows these four sections in the CFD boiler model, and the following paragraphs go into greater detail on each section. This boiler model was primarily used to analyze the effect that co-firing coal with biomass or natural gas had on  $\text{NO}_x$  emissions, but Zhang first created a baseline model simulating coal combustion to validate the geometry and CFD methods used in the simulation of the boiler. This baseline model was used as a starting point for further refinements and modifications in the simulation of coal combustion done in this thesis paper. Specifically addressed and tested in the improvement of this baseline model were problems involving high temperature regions, circulation zones, and large temperature gradients.

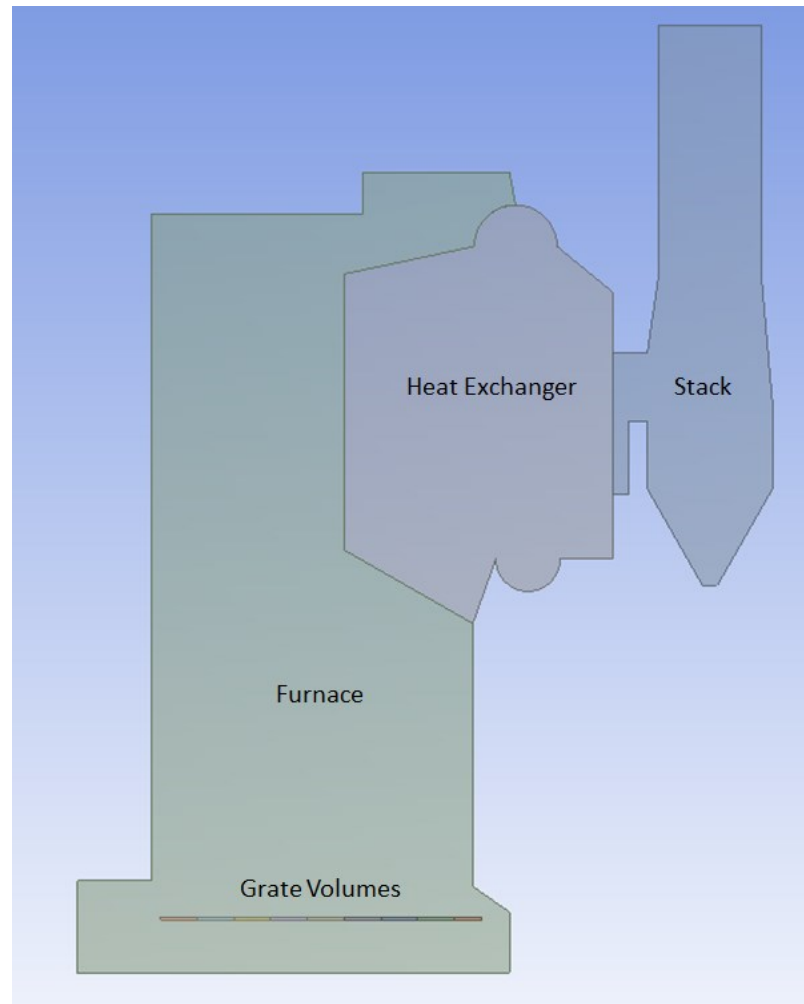


Figure 3.1. Previous Unit 10 geometry sectioning

### 3.1 Geometry and Mesh Grid

The geometry and grids for Unit 10 were created in the Gambit software. The real boiler has a very complicated geometry, including a moving fuel bed, heat exchanger water tubes, drums and superheaters. Simplifying the geometry down to the basic outer wall shape, with holes for the coal inlets and secondary air inlets, reduced the complexity



significantly. The inside of the boiler was left empty, but volumes were created representing the fuel bed, heat exchanger and stack regions. This simplified boiler geometry led to simpler meshing techniques and thus reduced computational time. Figure 3.2 shows an isometric view of the geometry with better visualization of the inlets and grate sections.

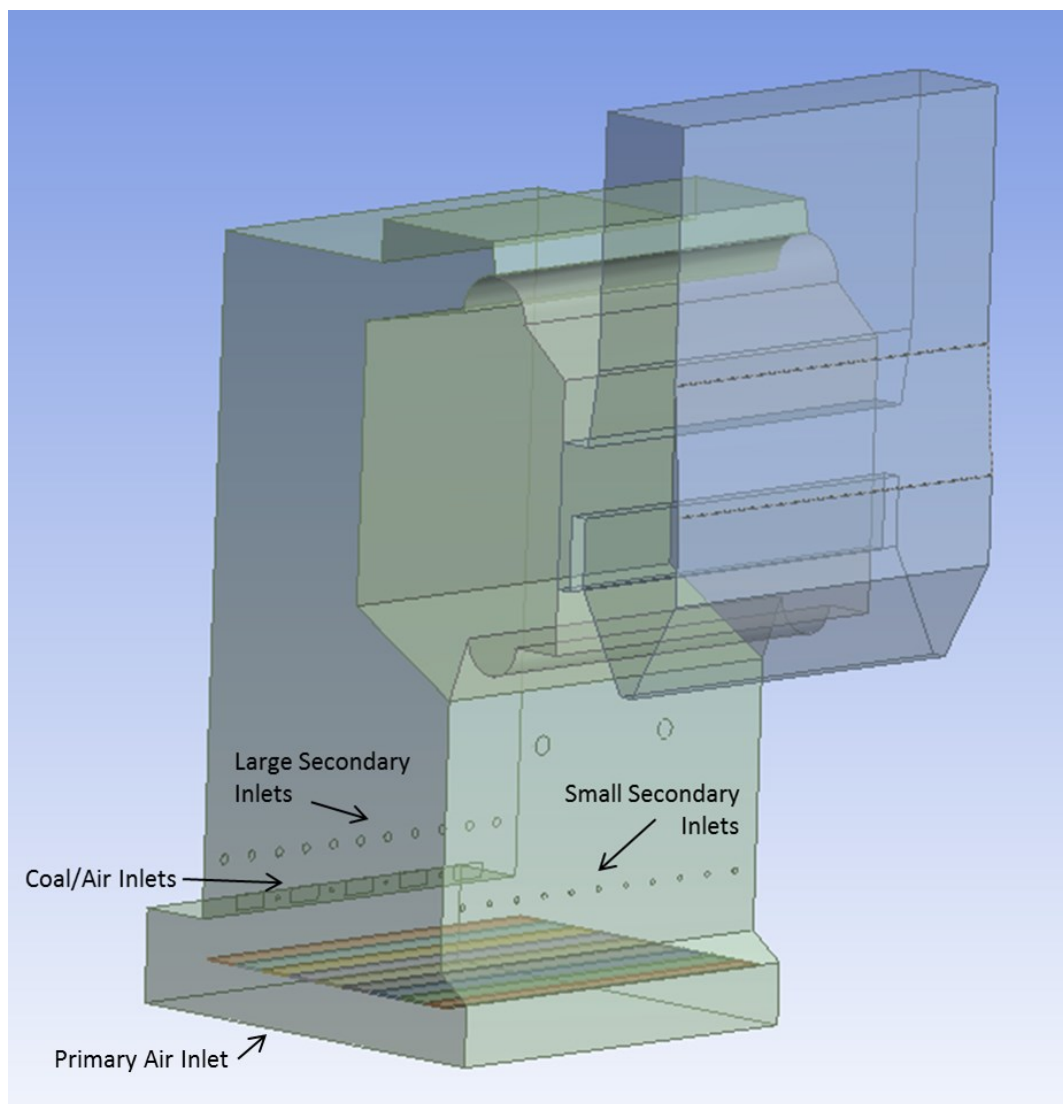


Figure 3.2. Isometric view of previous boiler geometry

Three different meshes were created, consisting of grids of approximately 630,000, 840,000 and 1,140,000 tetrahedral cells. A grid sensitivity analysis was run by the author and the second grid was chosen, based on its ability to provide accurate precision while still keeping the computational cost low. Figure 3.3 shows the final grid chosen for Unit 10, meshed in Gambit.

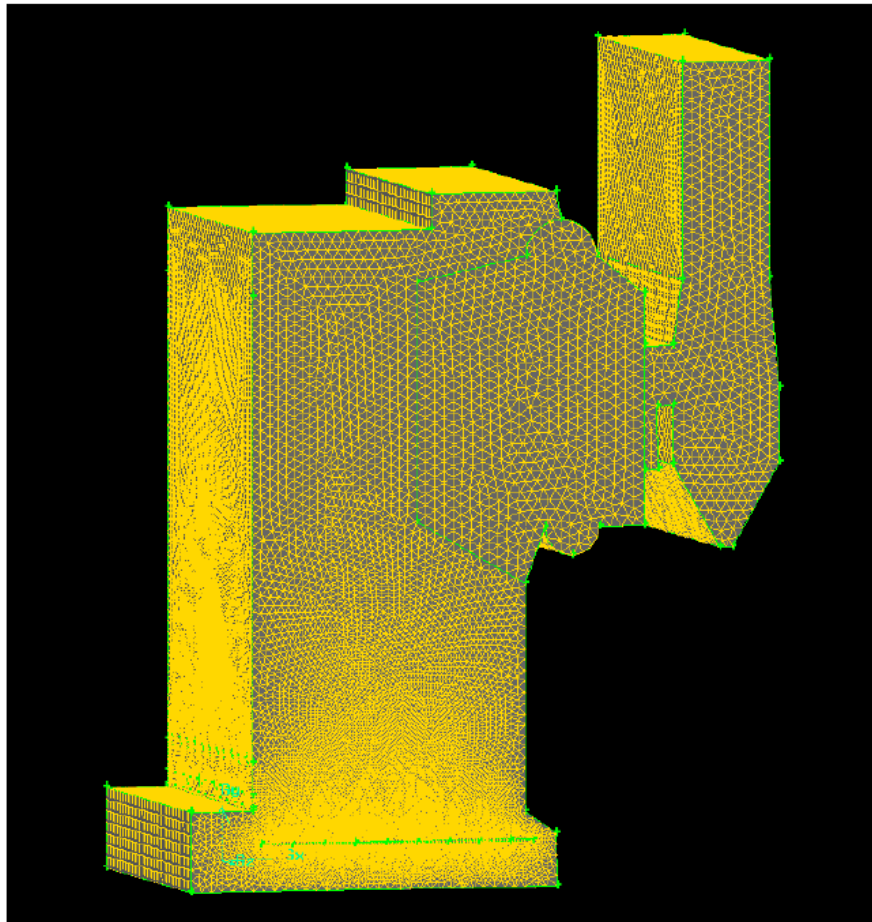


Figure 3.3. Previous Unit 10 boiler mesh grid

---

Source: Zhang 2011

### 3.2 Coal Analysis

The proximate analysis and dry, ash-free (DAF) ultimate analysis of coal used in the previous work are shown in Table 3.1, below. The Coal Calculator in Fluent used the mass fractions for DAF coal found in the ultimate analysis, while the mass fractions from the proximate analysis were used to calculate the mass flux distribution on the grate for the solid phase combustion approximation, discussed further in the next section.

Table 3.1 Coal analyses used in previous Unit 10 simulations

	Proximate Analysis [wt %]		Ultimate Analysis (DAF) [wt %]
Moisture	5.85	Carbon	72.4
Volatile matter	35.61	Hydrogen	5.07
Fixed Carbon	47.94	Nitrogen	1.64
Ash	10.6	Oxygen	8.26
Total	100	Total	100

Source: Zhang 2011

### 3.3 Coal Bed Model

As discussed in Chapter 2, one of the methods for fuel bed simulation is a two-dimensional model of the heat release and species flux from the grate. This allows the moving grate to be approximated as a steady state fixed bed with a fuel distribution vertically and horizontally. These distributions are essentially a representation of the physical process of the coal being thrown on to the grate, where it becomes unevenly distributed. The grate section in the previous model was split up into nine separate volumes in order to be able to create heat source and mass flux distributions along the

grate. The distribution of heat release along the nine grate zones that was approximated and used by the author is shown in Figure 3.3. The real boiler has a much more uneven distribution of coal, with some zones having a larger “pile” of coal or even none at all. A distribution this random is extremely complicated to model and thus the previous assumption was made to simplify and speed up the simulation.

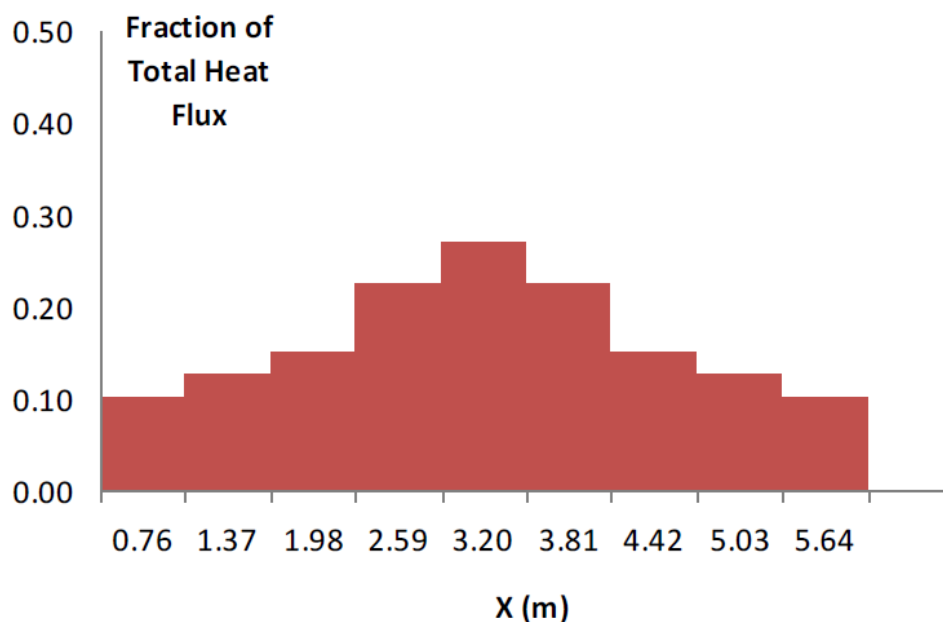
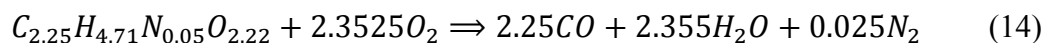


Figure 3.4. Grate heat flux distribution

---

Source: Zhang 2011

After the computations resulting in the mass fluxes of the species released from the bed during the solid combustion were completed, the volatiles above the bed followed a simple two-step reaction representing the gaseous combustion, given by Equations 14 and 15.



### 3.4 Boundary Conditions

The previous model used a primary inlet, small and large secondary inlets and the coal inlets for the air streams entering the furnace. Table 3.2 below shows airflow velocity values for air with a density of 1.225 kg/m<sup>3</sup> entering these inlets as well as the cross sectional area of each inlet.

Table 3.2 Air inlet boundary conditions for previous Unit 10 simulations

Inlet	Air Velocity [m/s]	Cross Sectional Area [m <sup>2</sup> ]
Large Secondary	17.8	0.200
Small Secondary	16.5	0.072
Primary	0.45	50.21
Coal	8.00	0.743

Source: Zhang 2011

These velocity values combined with the density of air gives a total air mass flow rate of 40.117 kg/s. This value is higher than the normal flow rate given by the UI power plant, leading to leaner combustion and overall lower furnace gas temperatures.

It was assumed that there was no conduction through the furnace walls, and they were given an emissivity of 1.0 and treated like a blackbody for radiation considerations. The outlet was defined as an outflow as opposed to the more common pressure-outlet condition. The temperatures for the walls and air inlet boundaries are shown in Table 3.3.

Table 3.3 Temperature boundary conditions for previous Unit 10 simulations

	Wall Temperature [K]		Air Temperature [K]
Furnace	850	Large Inlets	300
Slope	900	Small Inlets	300
Heat Exchanger	850	Primary Inlet	300
Stack	850	Coal Inlets	300

Source: Zhang 2011

### 3.6 Flow Models and Heat Exchanger

The CFD software Fluent was used for the simulation of the gaseous phase combustion and heat exchanger modeling in the Unit 10 boiler. Because of the nature of combustion and the speed of the air coming from the secondary inlets in the furnace, the Reynolds number can get as high as  $3e5$  (for the small secondary inlets), so a turbulent model was used to simulate the high speed and high temperature turbulent mixing of the gas phase combustion. The turbulent model used in this baseline coal combustion simulation was the realizable  $k - \epsilon$  model, the merits of which were discussed in Chapter 2. In addition to this, the P-1 radiation model was used, which expands the radiation intensity into orthogonal spherical harmonic waves. Because of the high speed and temperature of the combustion it was assumed that the overall reaction is controlled primarily by turbulent mixing, so the eddy dissipation model was used in the gaseous phase combustion to predict and model the rate of species production and mixing.

The heat exchanger in the real boiler is made up of drums that send water through tubes to take energy from the high temperature combusting flow, eventually evaporating into steam, which is then used to generate power. For the simulation, however, the tubes, superheaters and pipes were too complicated to model in the geometry. In addition, the

physics of the convective and radiative heat transfers from the gas to the water can get computationally expensive, so the heat exchanger was modeled as an empty volume. An energy sink was introduced in this volume and used to take out the amount of heat necessary to approximate the power that the real Unit 10 boiler generates. Since this baseline model was used to compare between pure coal combustion and combustion while co-firing coal and different biomasses, the bias error introduced by such a rough approximation of the heat exchanger did not affect the results in a significant way, as long as this baseline simulation resulted in reasonable and realistic temperature profiles and species concentrations.

### 3.7 Previous Unit 10 Simulation Results

Unit 10 has a working capacity of 2.58 kg steam per minute of operation, with a thermal efficiency of 82% for a full load of coal combustion. The baseline model in Zhang's thesis was used to simulate this condition. The author's convergence criteria – a constant temperature field and the balance of mass and energy – were met after around 9000 iteration steps. Figure 3.4 shows the temperature profile on a plane cut through the center of the boiler in the depth dimension. Figures 3.5 and 3.6 show the concentrations of O<sub>2</sub> and CO<sub>2</sub>, respectively.

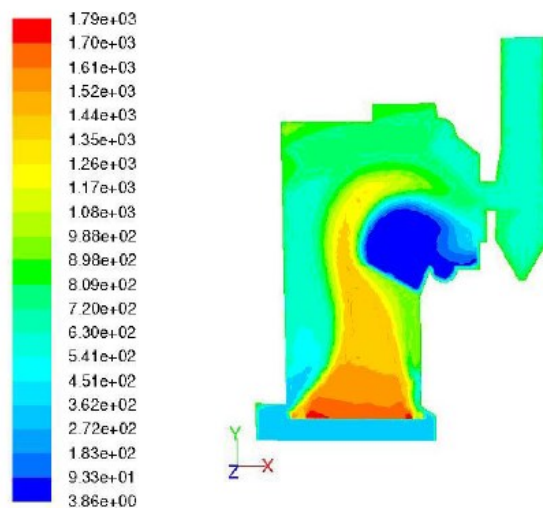


Figure 3.5. Temperature profile in the boiler

---

Source: Zhang 2011

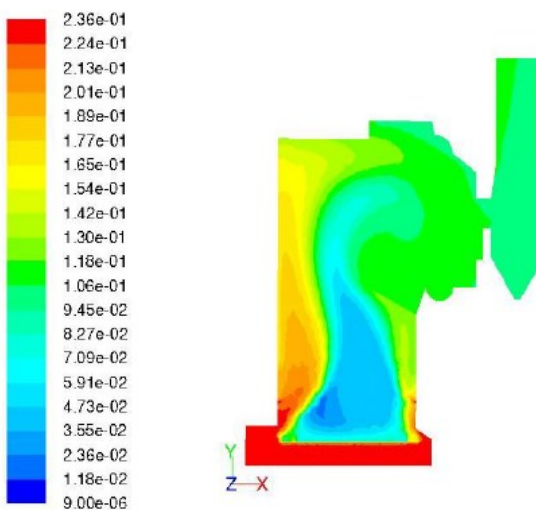


Figure 3.6. O<sub>2</sub> concentration profile

---

Source: Zhang 2011



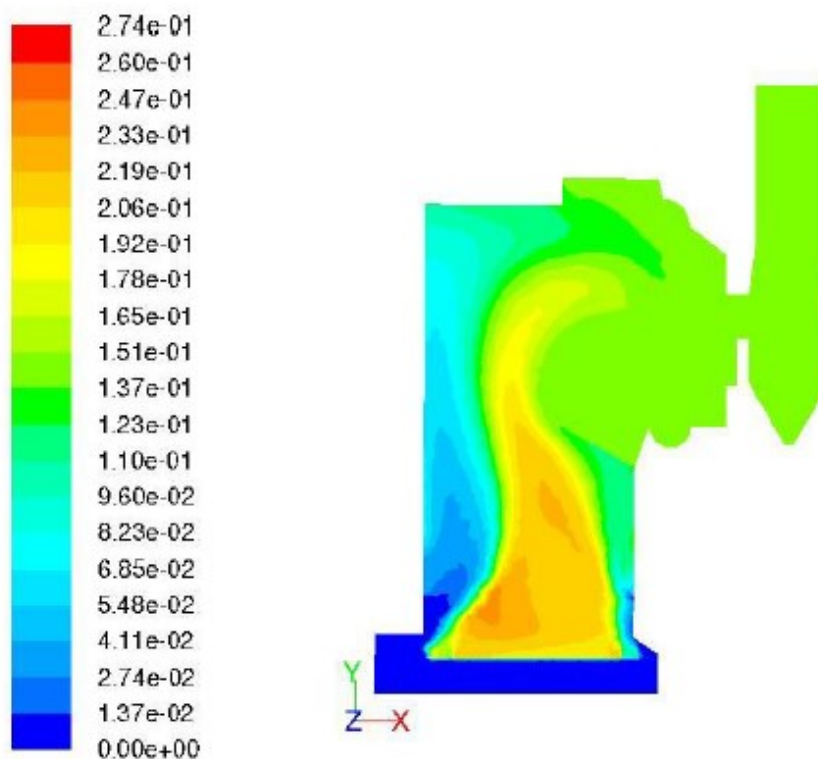


Figure 3.7. CO<sub>2</sub> concentration profile

Source: Zhang 2011

From the temperature profile, it is evident that the high temperature region is consistent with the bed model distribution: the temperature along the bed roughly matches the trend of the heat release distribution across the nine zones. The species concentration of oxygen in the furnace makes sense as well: there is a large depleted zone above the grate, corresponding to the modeled solid combustion on the bed, and the highest concentrations are found around the air inlets in the boiler. In a similar manner, the carbon dioxide concentration shows a large production zone above the solid coal combustion zone on the grate, and the concentration increases around the air inlets as secondary combustion produces CO<sub>2</sub> from the burning of the volatiles.

The simulation results for the gas temperature inside the boiler were compared to measured data at various windows along the furnace wall. There was some bias error present in the results for the temperature inside the boiler, but this was primarily due to the fact that the model was simulated with uniform coal distribution on the grate, while the real boiler has a much more random distribution of coal. However, the trends for the gas temperature followed the measurements fairly well and this was more important when comparing with the simulation of the co-firing of biomass with coal. Another simulation was run with a load of 2.00 kg steam per minute of operation, and the temperature trends again followed the measured data. For the purposes of the Zhang's thesis, the baseline model was determined to be satisfactory for making reasonable predictions of the effects of decreasing the coal load on the grate and co-firing with various biomasses (Zhang 2013).

## CHAPTER 4: CURRENT UNIT 10 BOILER MODEL

### 4.1 Coal Analysis

#### 4.1.1 Coal Properties

The bituminous coal used for all simulations done in the current research had a different composition than the one used in previous Unit 10 modeling. Table 4.1 shows the proximate analyses for both the coal and its DAF variant. The ultimate analyses for both were found and given in Table 4.2. In the same manner as in the previous model simulations, the species concentrations, heat flux values, and other properties relating to the solid coal combustion on the grate were found with calculations utilizing the proximate and ultimate analyses of the coal, and the Coal Calculator and Species Mixing functionalities in Fluent were used to determine the devolatilization process and the products resulting from the gaseous combustion above the bed.

Table 4.1. Proximate analyses of coal used in current Unit 10 simulations

	Proximate Analysis [wt %]	DAF [wt %]
Moisture	5.85	--
Volatiles	35.61	42.62
Carbon	47.94	57.38
Ash	10.6	--
Sum	100	100

Table 4.2. Ultimate analyses of coal used in current Unit 10 simulations

	Ultimate Analysis [wt %]	DAF [wt %]
Moisture	5.85	--
Carbon	68.16	81.58
Hydrogen	4.77	5.71
Oxygen	7.78	9.31
Nitrogen	1.54	3.4
Sulfur	1.3	--
Chloride	--	--
Ash	10.6	--
Sum	100	100

#### 4.1.2 Bed Model

The model used to determine the boundary conditions arising from the fuel bed after the coal devolatilization and solid carbon combustion was the same two-dimensional approximation used in the previous Unit 10 modeling. Although there are plenty of other bed models in literature (see Chapter 2), the scope of this research did not allow for modification of the bed model any more than selecting different properties of the coal. The previous boiler model fuel bed gave a fairly accurate approximation of coal being “thrown” on to the grate and burning, but simulations showed highly improbable temperature gradients and circulation zones in regions above the bed and in the heat exchanger region. For this reason, current research and simulations focused attention on developing a logical and realistic temperature profile in the boiler by modifying parameters and flow models in the furnace, heat exchanger and stack region, instead of fine-tuning the bed model.

## 4.2 Boundary Conditions and Flow Models

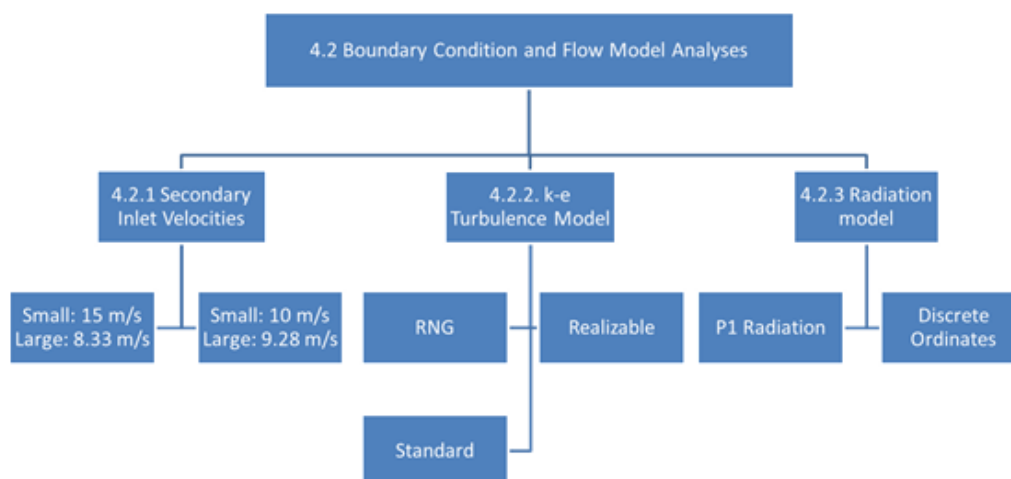


Figure 4.1. Flow chart for the simulations discussed in Section 4.2

After revising and performing the calculations relating to the coal chemistry and bed model heat and species concentration fluxes, various boundary conditions were changed in the Fluent simulation model to better reflect the real Unit 10 boiler operating conditions. The wall temperatures at points in the boiler (furnace walls, heat exchanger pipe walls, vent wall, stack walls, etc.) were updated to match the measured data provided by the power plant and a summary is shown in Table 4.3. The slope wall boundary condition was set to the “Coupled” option so that conduction could occur better through that wall. Based on the sizes of the primary and secondary air inlets and the mass flow rate of the air for a 100% boiler load condition, the air velocities for the various wall inlets were calculated, and specific values are listed in Table 4.4. The coal inlets were included because air enters with the coal being thrown onto the fuel bed.

Table 4.3. Wall temperatures of selected areas in the model

	Wall Temperature [K]
Furnace	673
Slope	--
Heat Exchanger	673
Pre-Stack Region	645.3
Stack	617.6

Table 4.4. Air inlet boundary conditions

Inlet	Air Velocity [m/s]	Cross Sectional Area [m <sup>2</sup> ]
Large Secondary	7.185	0.200
Small Secondary	21.25	0.072
Primary	0.3363	50.21
Coal	1.98	0.743

#### 4.2.1 Turbulence Model

As discussed in previous chapters, one of the most important considerations when doing this type of combustion modeling is the turbulent behavior of the superheated gas flow. Chapter 2 described some different models used by researchers when doing boiler modeling and outlined the theory of the  $k - \varepsilon$  turbulence model, one of the most common turbulent flow models. The previous Unit 10 boiler simulations used the realizable  $k - \varepsilon$  model, so it was used as the starting point for the current work. Figure 4.2 shows the temperature profile for a simulation based on Zhang's 100% coal combustion case, with the only modifications being ones discussed up to this point. The velocity vectors are seen in Figure 4.3, and they show the main flow path of the gas. It is clear from the

temperature and velocity data that the high ratio of the small secondary inlet velocity (right side, or front wall) to the large secondary inlet velocity (left side, or back wall) is causing an imbalance of high temperature zones in the middle furnace region where the secondary (gaseous phase) combustion occurs. The circulation in the heat exchanger is evident in both figures as well, as there are large temperature gradients and the velocity vectors drop in magnitude significantly before reaching the stack volume.

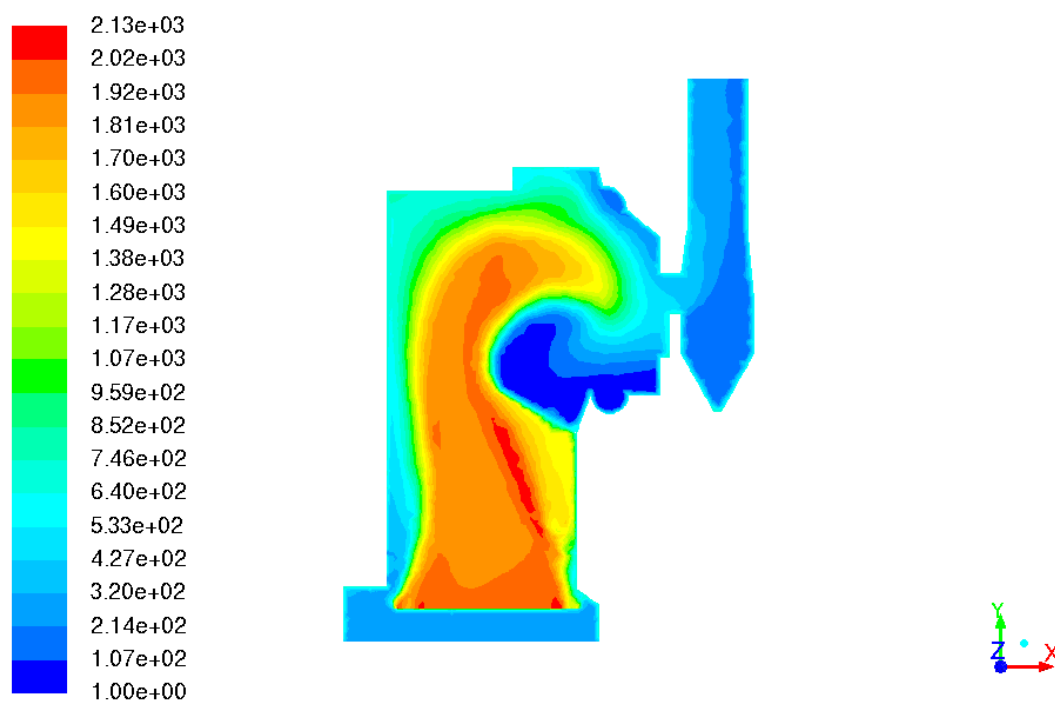


Figure 4.2. Temperature profile for initial simulation of current model

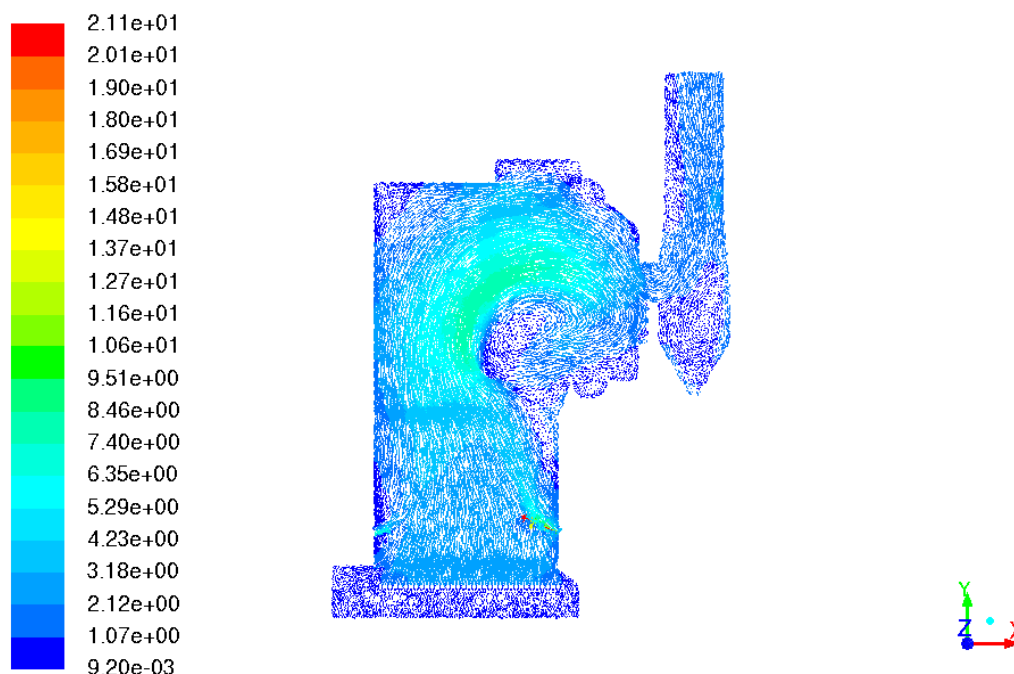


Figure 4.3. Velocity vector profile for initial simulation of current model

Though not discussed in the literature portion of this paper, the RNG  $k - \varepsilon$  turbulence model was tested in a boiler simulation. Fluent documentation summarizes the advantages and common uses of the RNG model: it is more accurate for rapidly strained flows, enhances accuracy for swirling flows, and can account for low Reynolds number effects. Figures 4.4 and 4.5 show the temperature profile and velocity vectors, respectively, after 20,000 iteration steps. The conservation equation residuals for the simulation showed very poor oscillatory convergence, with large amounts of noise and high peaks at random periods during the simulation time. As evident from the figures, the flow path is not very clear or logical, and the temperature profile has unrealistically high magnitudes and is not fully propagated throughout the entire boiler. The unsatisfactory results from the use of this model are most likely due to poor wall treatment, and



considering that low Reynolds number effects are most prominent at the walls, this treatment affected the RNG model alone out of the three turbulence models. According to Fluent documentation, the RNG model is more reliable for a wider class of flows than the standard  $k - \varepsilon$  model, but in the case of the current simulations, the realizable model gave a decidedly more accurate representation of the gas flow in the boiler.

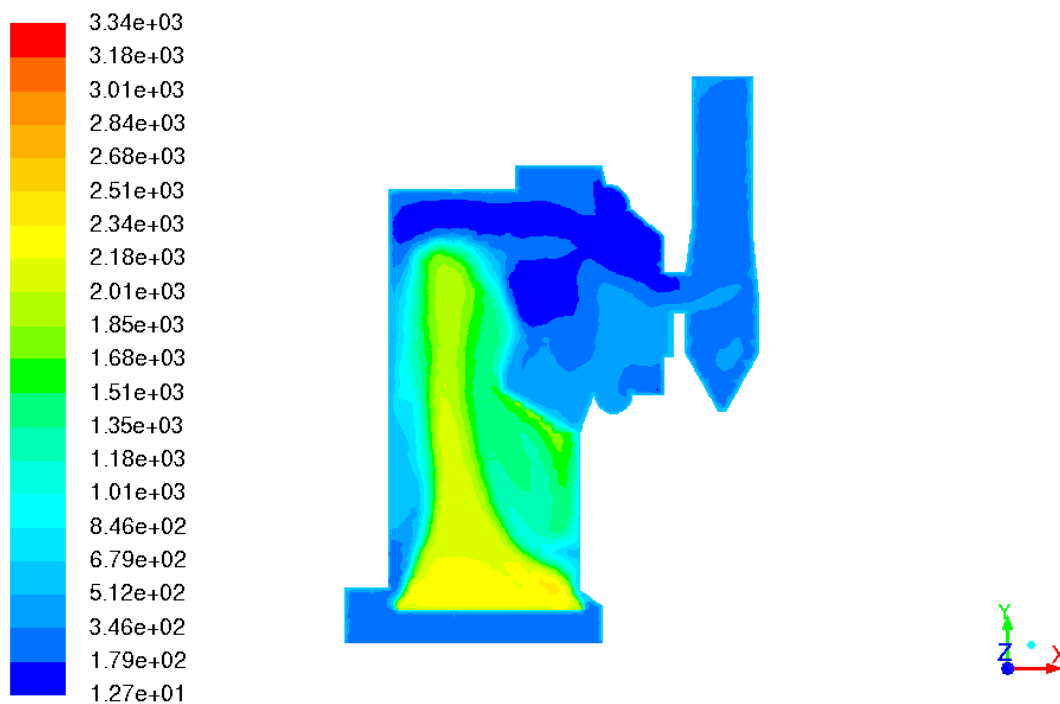


Figure 4.4. Temperature profile using RNG turbulence model

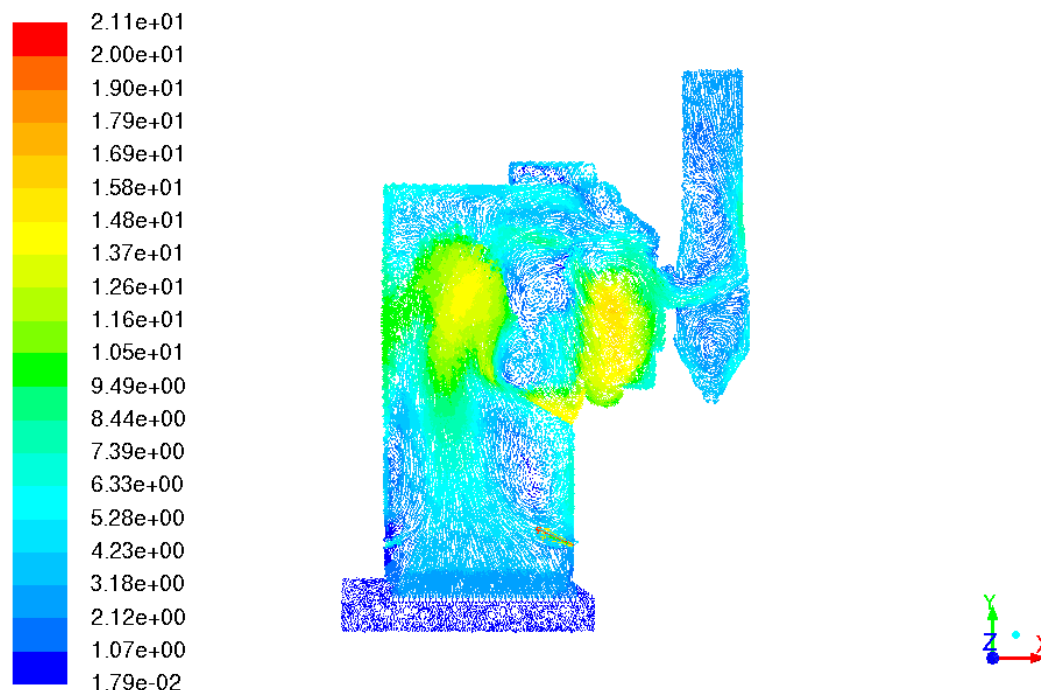


Figure 4.5. Velocity vector profile using RNG turbulence model

The standard  $k - \varepsilon$  turbulence model was also used in a simulation to determine any observable differences between it and the realizable model. Figures 4.6 and 4.7 show the temperature profile and velocity vectors respectively. After running the simulation with the standard turbulence model it was noted that the circulation in the heat exchanger region was more pronounced. The velocity vectors clearly show two separate flow paths: one rotating in the heat exchanger and one going out through the stack. The temperature profile shows this as well, and the circulation is more fully developed than in the profile resulting from the realizable model (Figure 4.2). Another important distinction between the two models is that the maximum temperature in the boiler using the standard model is much higher and takes up noticeably more space in the furnace volume. In contrast to the realizable model, the standard model does not seem to give any indication that the

secondary inlet velocities are affecting the turbulent mixing or secondary combustion of the gas in a significant way. Based on these observations, it was assumed that the realizable  $k - \varepsilon$  model was able to handle the physics of highly turbulent flows as well or better than the standard model, especially for channel and rotating flows, both of which are present in the boiler simulation. This conclusion agrees with  $k - \varepsilon$  model theory and validation done by researchers (discussed in Chapter 2) and for this reason the realizable model was set for all subsequent simulations.

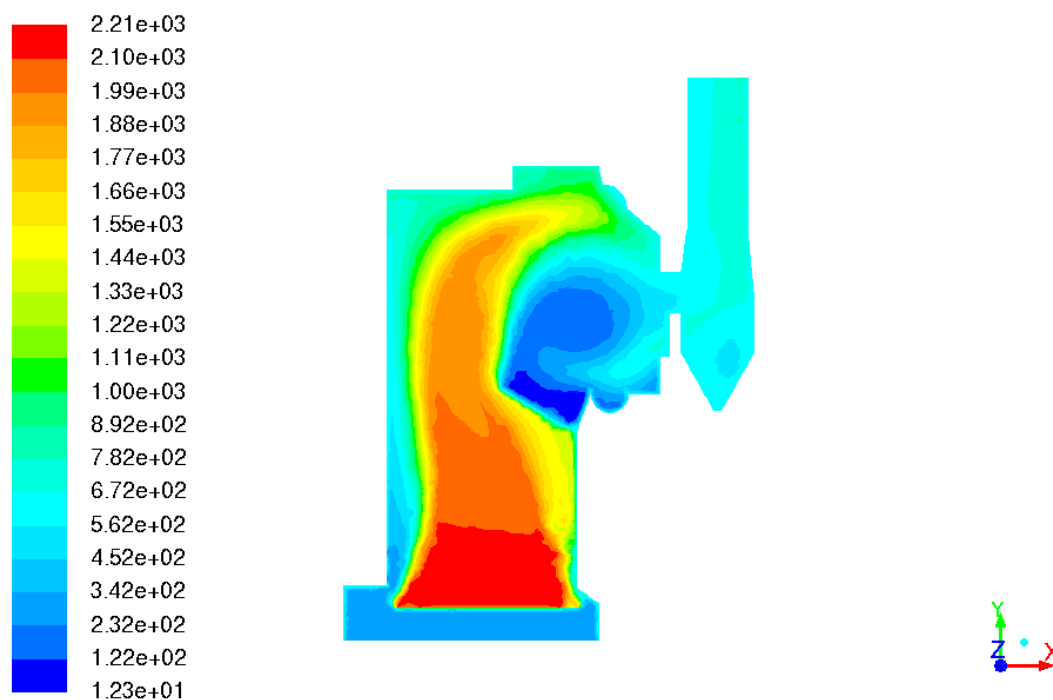


Figure 4.6. Temperature profile using standard turbulence model

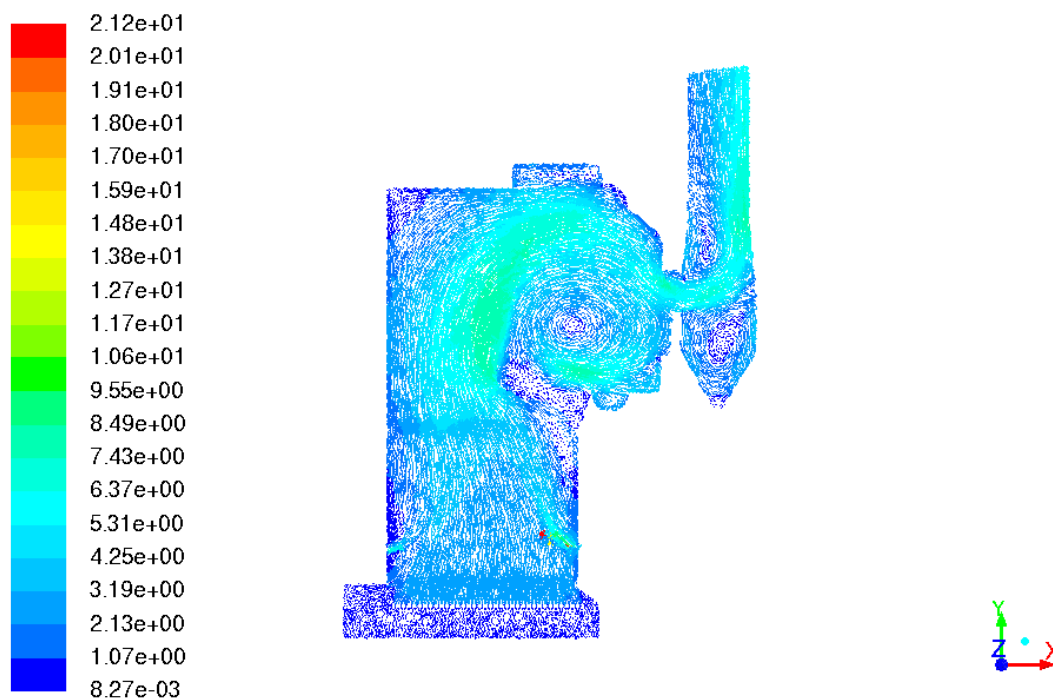


Figure 4.7. Velocity vector profile using standard turbulence model

The species production and mixing, which is coupled to the turbulent flow, was calculated using the eddy-dissipation model. Lightly touched upon in Chapters 2 and 3, the eddy-dissipation model is accurate for high velocity and temperature flows and assumes that species production and mixing is primarily controlled by turbulent mixing. Both of those conditions (high velocity and high temperature flow) were met for the coal combustion simulations and Zhang's results showed no problems with the model, so it was set for all simulations in the current Unit 10 modeling work.

#### 4.2.2 Radiation Model

Another flow consideration necessary for the model simulation was the treatment of radiation heat transfer in the furnace. The majority of research studied in Chapter 2

shows that most simulations were run using the discrete ordinates radiation model. The main reason for this is that many of the boiler simulations included discrete phase modeling or some type of particulate analysis, and the discrete ordinates model is well suited for particulate effects and localized heat sources. However, Zhang's coal model (Chapter 3) did not include any particulate coal or discrete phase modeling so the P1 radiation model (the simplest Fluent radiation model) resulted in reasonable temperature profiles and gradients in the boiler furnace area. As a result, in the same manner as the testing of turbulence models, the previous boiler radiation model was used as a starting point for the current simulations. Since the turbulent models and radiation models could be tested simultaneously, Figure 4.2 shown in the previous section displays the temperature profile for a simulation using the P1 radiation model and the realizable  $k - \varepsilon$  model. Considering that the only settings changed in the model versus the previous Unit 10 model were those relating to the coal calculations, the temperature profile is fairly similar to Zhang's results.

A simulation was also run using the discrete ordinates radiation model because of the success of the model in other boiler simulation research cases, as briefly discussed in Chapter 2. Although there is no particulate modeling in the current simulations, the energy source terms present in the grate and heat exchanger sections of the boiler led to the assumption that the discrete ordinates model may be able to resolve these localized heat sources better than the P1 model. Figure 4.8 shows the temperature profile in the boiler after a simulation using the discrete ordinates model and realizable  $k - \varepsilon$  model. While there are no obvious problematic areas like in the RNG turbulence simulation, the overall maximum temperature is higher and more spread out than when using the P1 model. In addition, the high temperature regions are in the areas of the furnace above the secondary air inlets and near the top wall, when they should be nearer to the bed.

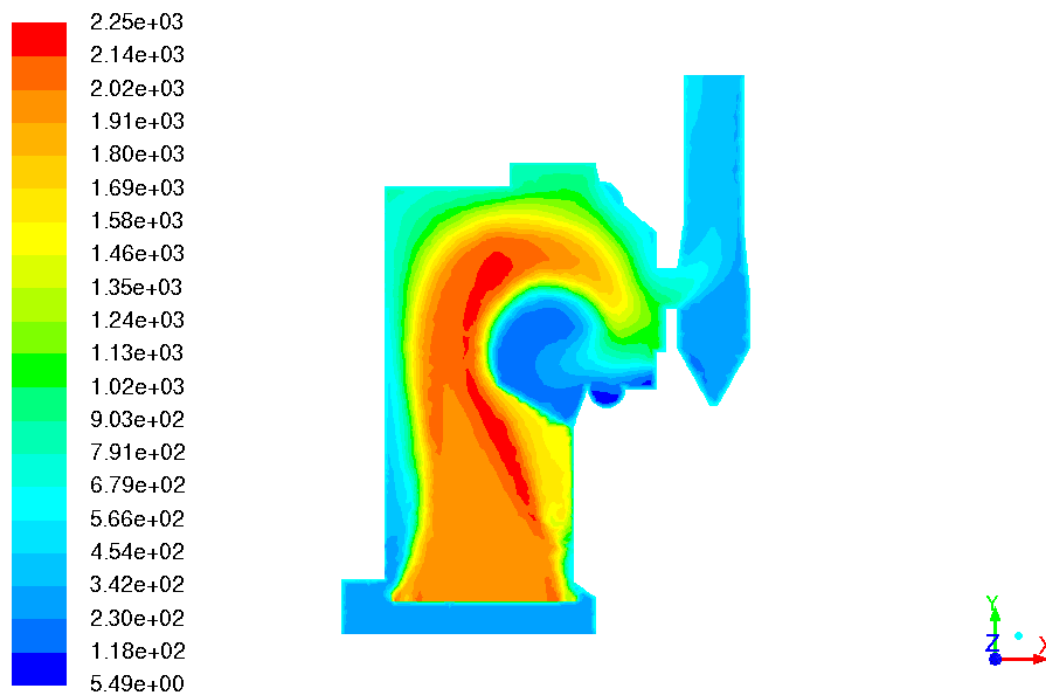


Figure 4.8. Temperature profile using discrete ordinates radiation model

As a result of the simulations and tests detailed above, all further simulations used the realizable  $k - \varepsilon$  turbulence model and the P1 radiation model for the analysis of the turbulent gas flow and the radiation heat transfer in the gas, respectively. The realizable model handles the circulation well and the P1 model gives an accurate approximation of the radiation in the furnace.

#### 4.2.3 Inlet Velocities

The final modification made to the boundary conditions in the model was the varying of the secondary inlet velocities in an attempt to reduce or eliminate the high temperature regions present at the inlet locations. Table 4.4, in the previous section, listed the values used for the air velocities at the various inlets in the furnace walls for all of the

simulations run up to this point. The first modified simulation run was with a small secondary inlet velocity of 15 m/s. The corresponding large inlet velocity was calculated to be 8.35 m/s in order to keep the mass flow rate of the air into the furnace constant. After comparing the resulting temperature profile (Figure 4.9) to the temperature profile from the original velocities (Figure 4.2), the assumption that lower air velocity would reduce the high temperature region near the small inlets was found to be good. In order to further validate this assumption another case was run, this time with a small inlet velocity of 10 m/s and a corresponding large inlet velocity of 9.28 m/s. The temperature profile, given in Figure 4.10, again showed that the reduction in velocity led to lower magnitude high temperature regions near the inlets. The average reduction in temperature between the 15 and 10 m/s velocity cases in these zones was 2111 K to 2016 K (4.5%), which may also mean a small abatement in NO<sub>x</sub> production.

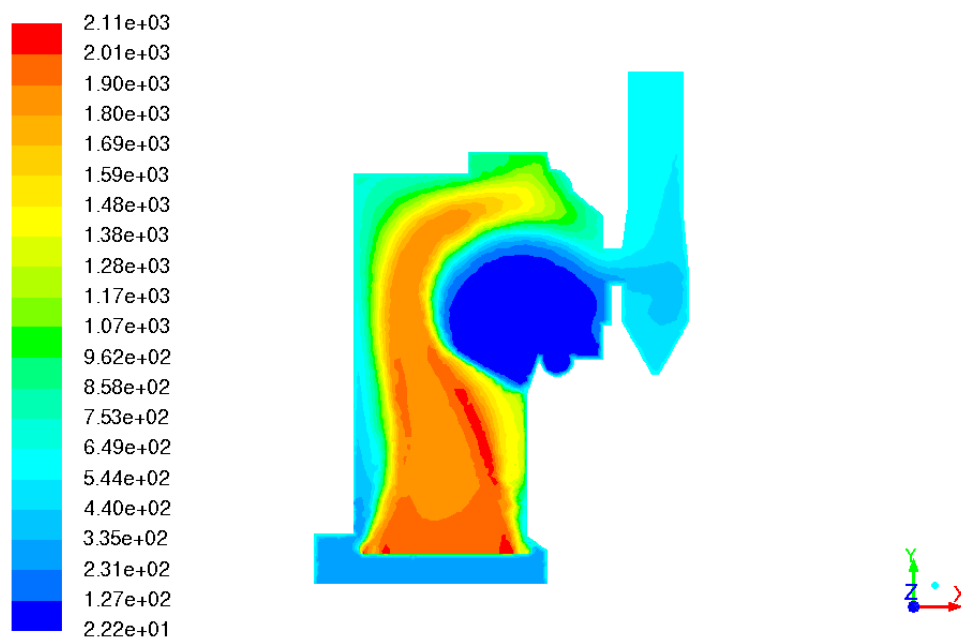


Figure 4.9. Temperature profile for 15 m/s small inlet velocity boundary condition

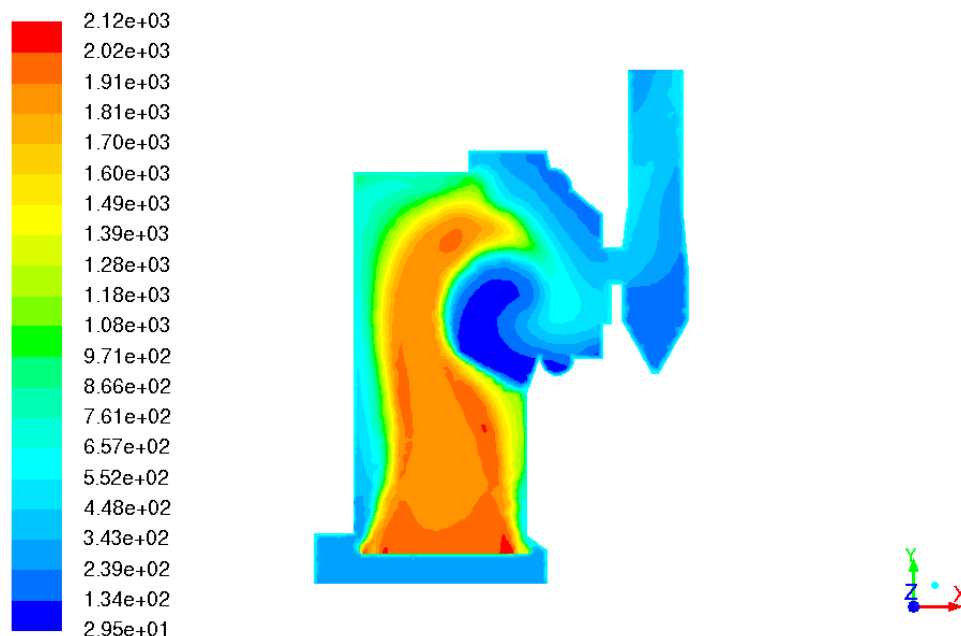


Figure 4.10. Temperature profile for 10 m/s small inlet velocity boundary condition

One thing to note about the high temperature region near the inlets is that at first glance it does not seem to agree with the behavior of combusting gases. In general, adding air to hydrocarbon combustion will lower the temperature as the mixture becomes fuel-lean. The maximum temperature occurs near the stoichiometric mixture point, and the temperature lowers again as the mixture becomes fuel-rich. In the case of this model, the large magnitudes of the heat flux and gaseous hydrocarbons released from the grate, combined with the air coming in from below (which does not consist of the total amount of air mass flow into the furnace), results in a simulated fuel-rich mixture. When the rest of the air mass flow comes into the furnace via the secondary inlets, the mixture nears its stoichiometric ratio and therefore the combustion temperature increases in these “stoichiometric zones”.



Even though the simulations showed a trend of reducing high temperature regions with decreasing small secondary inlet velocity, the slower the air speed became, the further the model parameters were from measurements taken at the power plant. Some future simulations used the modified velocity values because of the promising results, but otherwise the velocities were restored to their original values for all cases.

### 4.3 Geometry and Mesh Grid

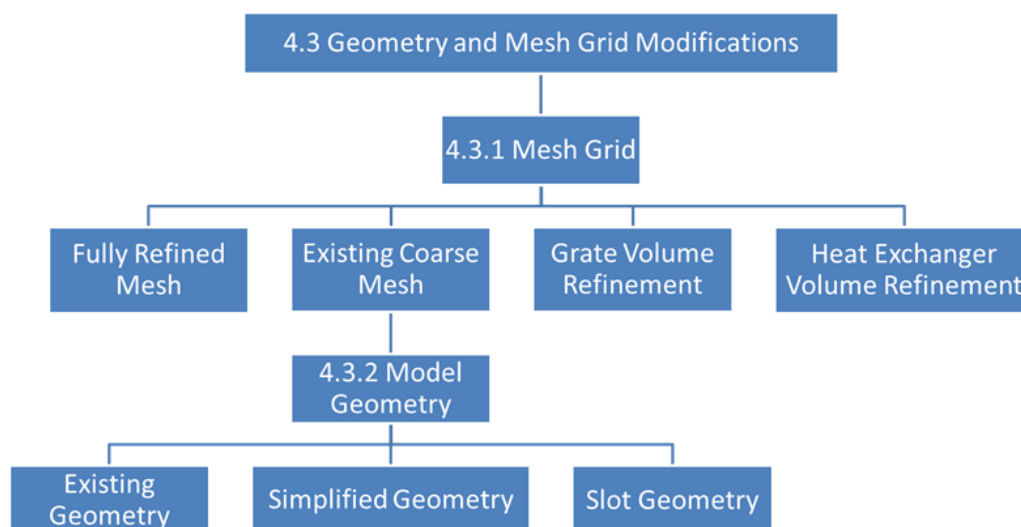


Figure 4.11. Flow chart for the simulations discussed in Section 4.3

The issues in the heat exchanger were also addressed by modifying the mesh grid and geometry of the boiler. The old model was broken up into volumetric sections for the grate, furnace, heat exchanger, and stack only, as seen previously in Figure 3.1. To create the option for more section-specific meshing techniques, the furnace volume was broken up into three parts: the furnace inlet section, encapsulating the grate volumes and the primary air inlet, the middle furnace section, containing the coal inlets and all of the

secondary air inlets, and the upper furnace section, which interfaces with the heat exchanger volume. Figure 4.12 shows this updated geometry.

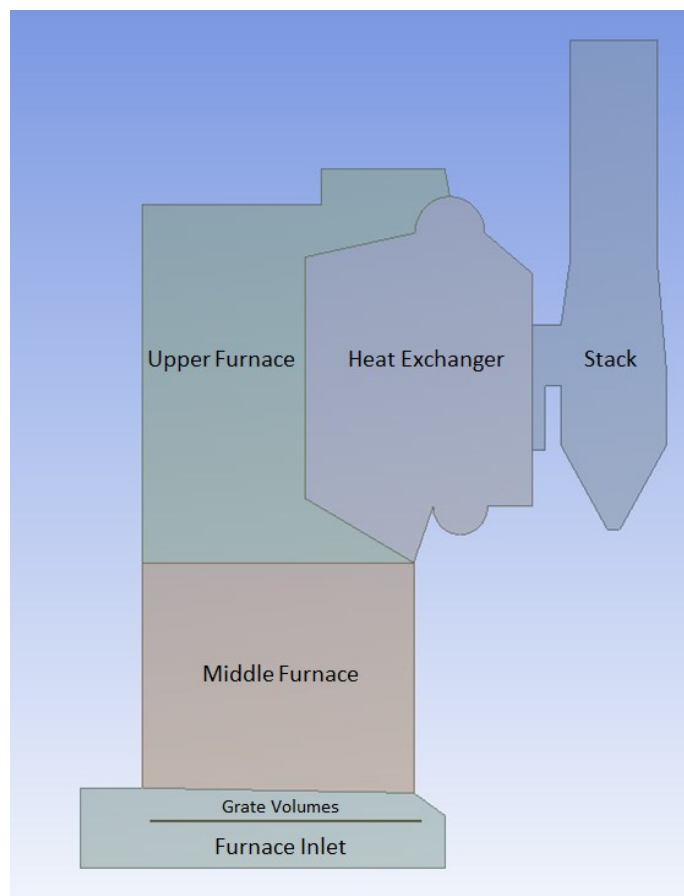


Figure 4.12. Modified geometry used in current Unit 10 simulations

### 4.3.1 Mesh

Using the new geometry, different mesh sizing was compared, including refined mesh for all sections, coarsening for all sections, and specific section refinement. Table 4.5 gives a summary of the different mesh sizing methods, their simulation performance and total number of element nodes. The simulation performance was based on the usage of eight CPU cores in parallel processing and the total number of nodes is the value reported from the Fluent software.

Table 4.5. Mesh sizing techniques, their performance and number of element nodes

	Simulation Speed [iterations/minute]	Total Number of Element Nodes
Fully Refined Grid	2.34	1222454
Refined Grate Volumes	9.10	371399
Refined Heat Exchanger Volume	18.38	171321
Fully Coarse Grid	26.44	115589

For the purpose of comparing different meshes, the model settings resulting from the boundary condition testing and simulations in Section 4.2 were used. The finest grid, with 1.2 million nodes, resulted in a very slow average simulation time. However, the results showed a temperature profile almost exactly identical to the one obtained from simulations with the Zhang's final mesh size (Figure 3.5). With no apparent improvement in the temperature distribution in the furnace, and a large computational cost, the fully refined mesh was abandoned for the rest of the current simulation work.

The next modification primarily attempted to reduce the high temperature zones directly on and above the fuel bed by keeping the refined mesh on the grate volumes while the rest of the model grid was returned to the original size. The boundary conditions resulting from the fuel bed were based off very simplified reaction

calculations and heat flux and species flux distributions (see Chapter 3), so this mesh modification also served to determine the effect that refinement had on the grate's temperature distribution. Using this model mesh, simulations ran almost four times faster than the previous grid analysis, but results showed a temperature distribution above the grate (Figure 4.13) that was not noticeably different than the one from the fully refined grid or the original grid. For this reason, the refined grate mesh was also eliminated.

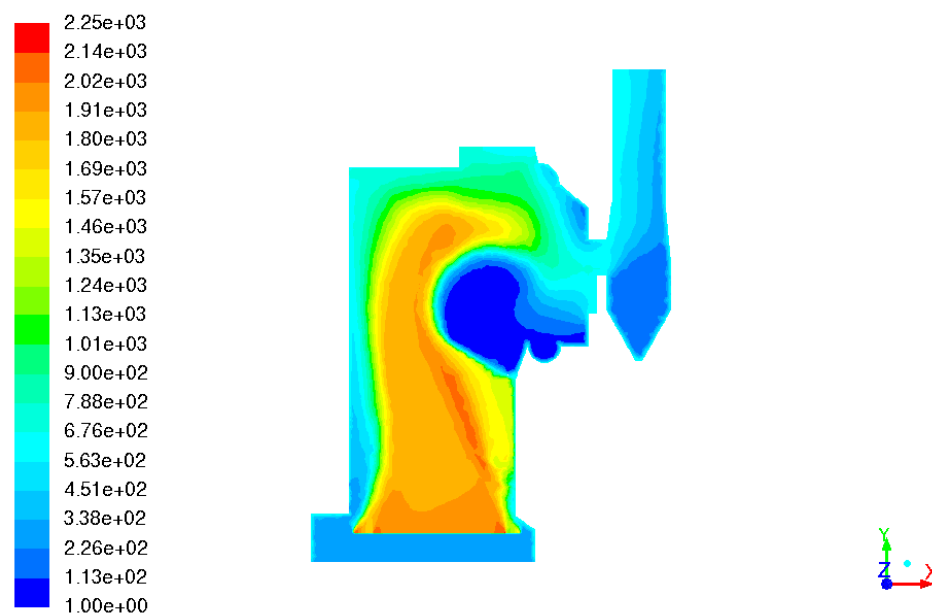


Figure 4.13. Temperature profile using a refined grate mesh grid

In order to better resolve the large temperature gradients resulting from the circulation in the heat exchanger volume, the entire model was returned to the original grid size except for that specific section, which was refined. The average simulation time using this mesh was still fairly fast (18.38 iterations/minute versus 26.44

iterations/minute for the fully coarse mesh) but the circulation was not improved enough to justify a slower computation time than the coarser full model mesh. Figure 4.14 below shows a comparison of the temperature profile between the mesh with the refined heat exchanger volume (left) and the fully coarse mesh (right). While the temperature gradients were indeed slightly improved, the temperatures inside the heat exchanger volume were still highly unrealistic. Going forward, the mesh size used for all subsequent models was the coarser mesh with uniform size across all geometric sections.

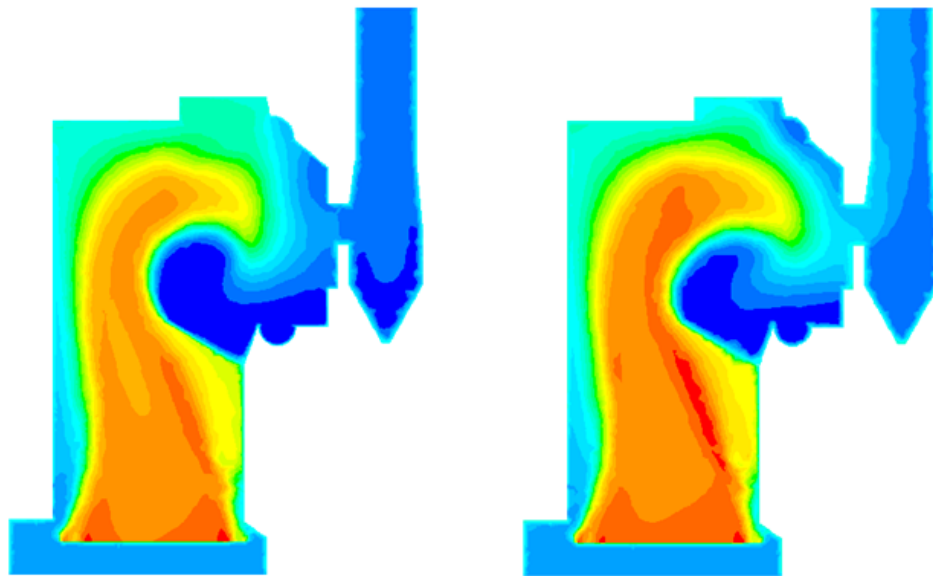


Figure 4.14. Comparison of the temperature profile between models with a refined heat exchanger mesh grid (left) and without (right)

### 4.3.2 Geometry

With a base grid size chosen, the next step was to make geometric modifications in a continued effort to reduce circulation zones and soften high temperature gradients without making specific changes to the chemical or mathematical models. From examination of temperature profiles from previous simulations (Figures 4.2, 4.6, 4.9, 4.10 and 4.13), it was evident that most of the circulation and low temperature zones appeared in the bottom of the heat exchanger volume and the bottom of the stack section. Using this information, the geometry of the boiler was simplified to the essential sections, removing the large water tank cylinder section and the bottom of the stack (which is only used in the real boiler to catch ash and soot). Figure 4.14 below compares the original geometry with this simplified representation. After running simulations with this reduced geometry (see Figures 4.16 and 4.17), circulation was still observed in the bottom of the pipe volume, and although the low temperature zone was eliminated from the stack, the continued presence of unrealistic temperatures in the heat exchanger volume made it evident that the underlying problems with the boiler model were not due to the geometry in any significant way. In addition, Figure 4.17 shows a flow path that got more unrealistic when compared to simulations with the original geometry.

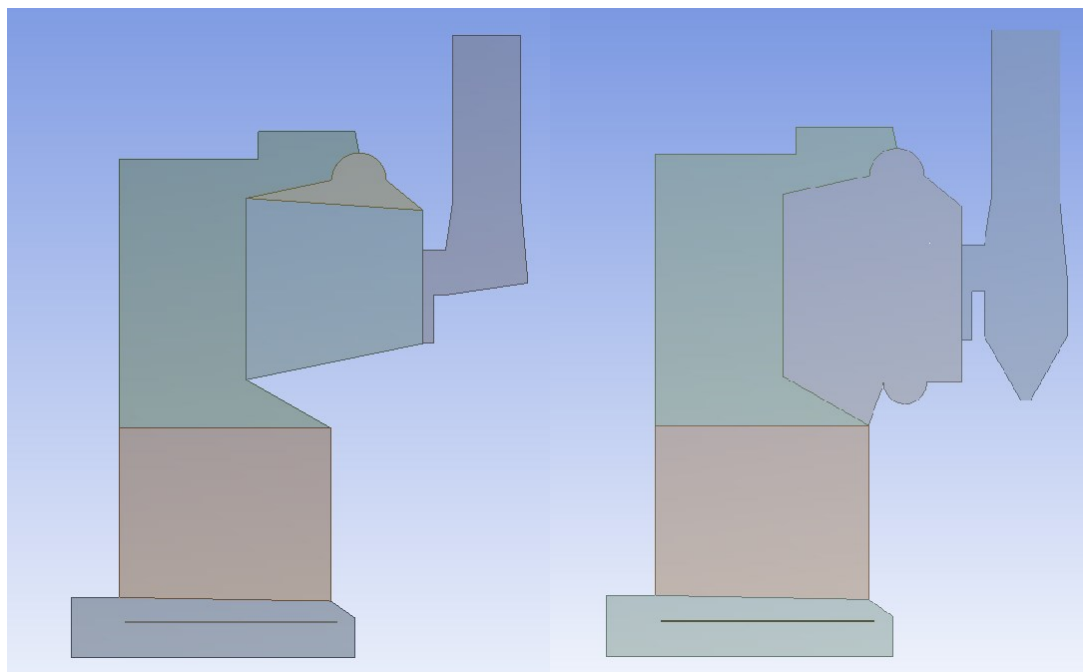


Figure 4.15. Comparison reduced geometry (left) and original geometry (right)

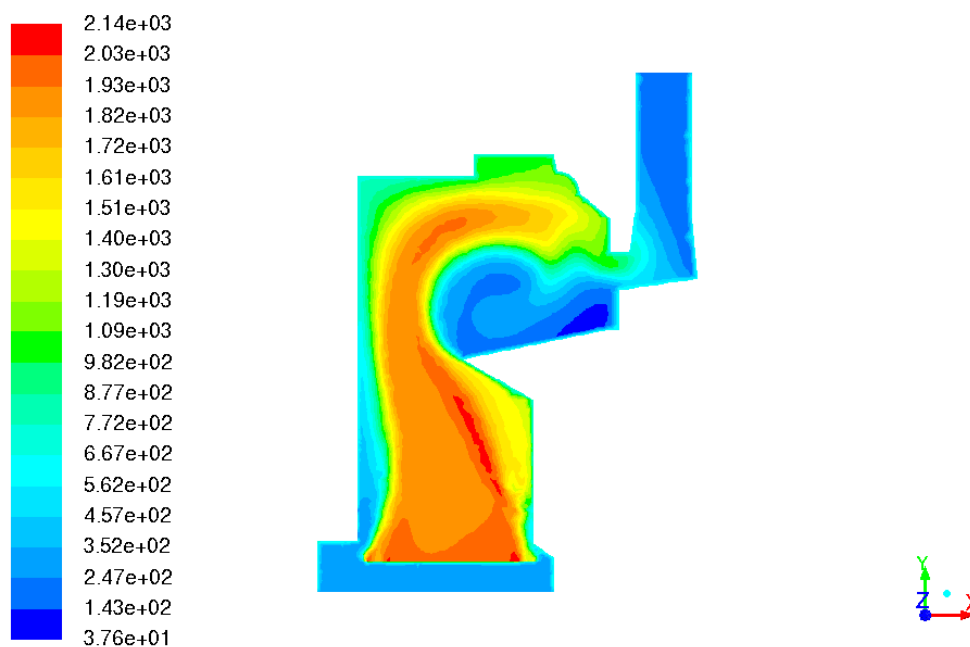


Figure 4.16. Temperature profile using reduced geometry

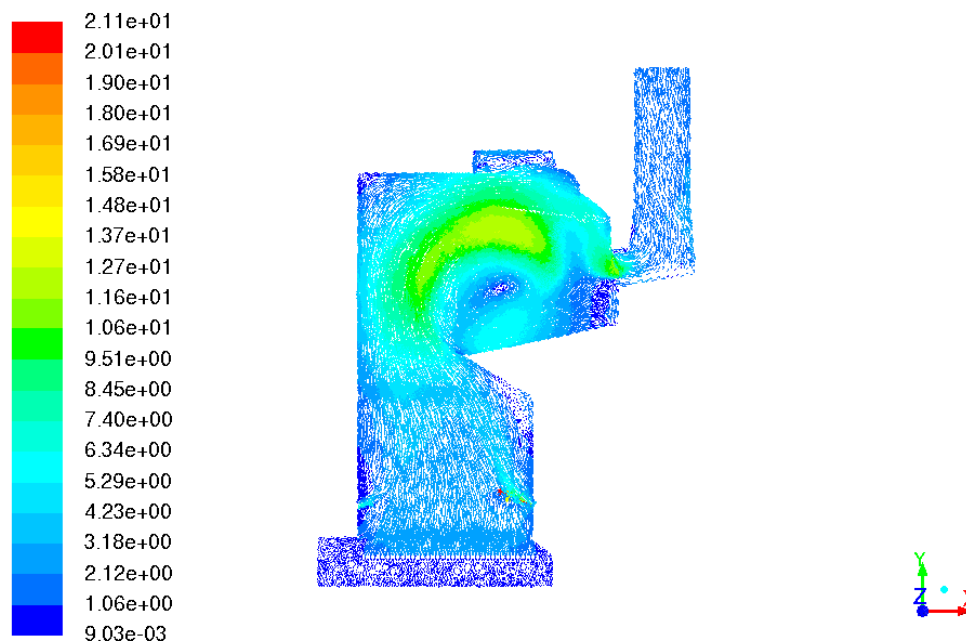


Figure 4.17. Velocity vector profile using reduced geometry

Another observation made from Figure 4.16 was that the highest temperature gradient goes across the slope wall into the bottom of the heat exchanger volume. The real boiler will have some conduction through this steel wall into the heat exchanger section, while in the simulations none seemed to be occurring, even with a wall thickness and thermal conductivity specified in the boundary conditions. In order to study how Fluent was treating this wall during the simulation, slots were made in the slope wall (circled region in Figure 4.18) and more simulations were run. It is clear from Figure 4.19 that with these slots present, circulation in the bottom of the exchanger reduced significantly. This was a fairly predictable result because the slots were essentially “forcing” Fluent to reduce this large temperature gradient by creating a secondary flow path that cut through the pipe volume. Without the slots, the high velocity secondary air inlets forced the main flow path quickly along the slope wall and up around the division between the upper furnace and heat exchanger volumes. This high speed flow prevented



efficient conduction through the slope wall and caused the high velocity streamlines to “shoot out” toward the stack after entering the heat exchanger volume. Although the slotted geometric modification resulted in simulations that showed a more realistic temperature gradient, the modification in itself was not a good representation of how the real boiler looks and handles a high speed flow. The low temperature zones that continued to remain also showed that this modification was not an effective solution to the unrealistic temperature profile.

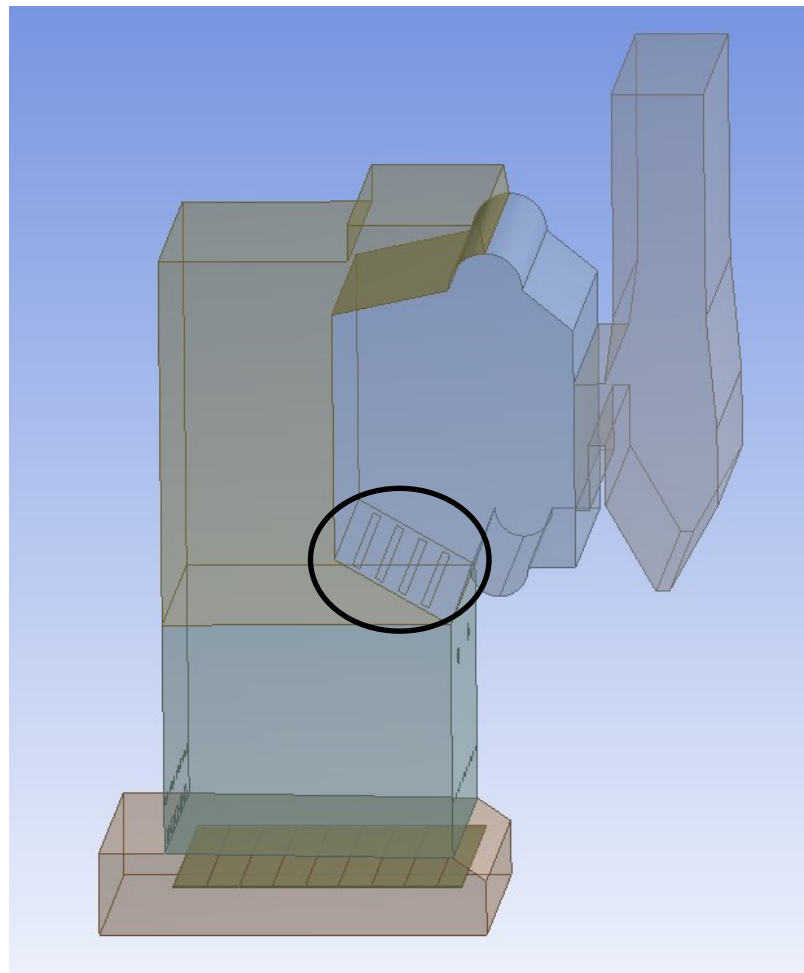


Figure 4.18. Boiler model with slotted slope geometry

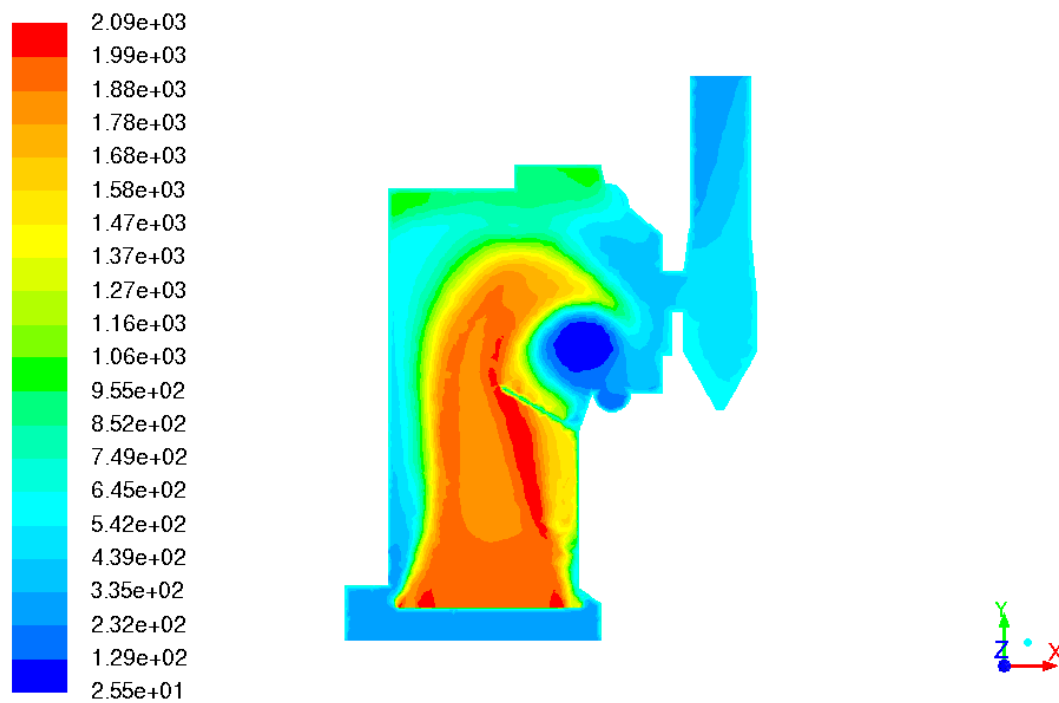


Figure 4.19. Temperature profile using slotted slope geometry

## 4.4 Heat Exchanger Modifications

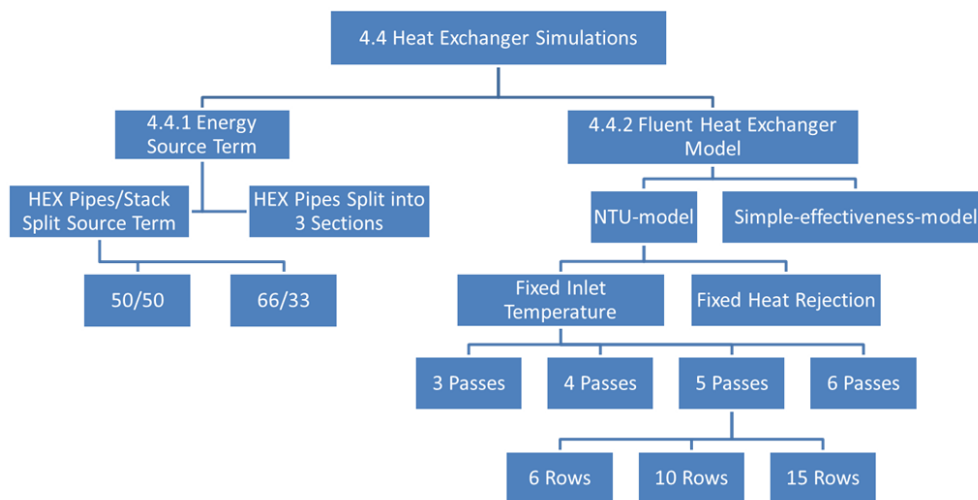


Figure 4.20. Flow chart for the simulations discussed in Section 4.4

With almost all of the geometric and grid modifications either having no effect on the flow path or not realistically improving the temperature profile in a significant way, other options needed to be explored to fix the problems in the heat exchanger and stack volumes.

### 4.4.1 Energy Source Terms

The existing boundary conditions specified that all of the heat that the real boiler produces to create a full load of steam is removed in the model by a negative energy source term in the heat exchanger volume. It was assumed that because of this simplification, the easiest way that Fluent's source models can resolve this large energy

loss from the flow is to create significant temperature gradients in the area, leading to large circulations and impossible temperatures (i.e. 1 – 100 K). Different modifications were made to the boundary conditions governing the negative source term for two reasons: to observe the effect that this source term has on the temperature gradients and circulation in the model, and to attempt to reduce the magnitude of both phenomena, resulting in a more realistic simulation.

Since the entire source term was localized to the heat exchanger volume, it was assumed that this localization contributed to the large temperature gradients and intense circulation present. For this reason, the negative energy source term was split across the heat exchanger volume and the stack volume. The first simulation was run with two-thirds of the energy being removed in the heat exchanger volume and the remaining amount taken out in the stack section. The results of the simulation showed that even though the circulation was reduced in the pipe region, the low temperatures were still unrealistic. In addition, a low temperature region appeared in the bottom of the stack volume, showing that circulation was also occurring there as a result of the negative energy source term. Figure 4.21 shows the temperature profile in the boiler after 30,000 iterations.

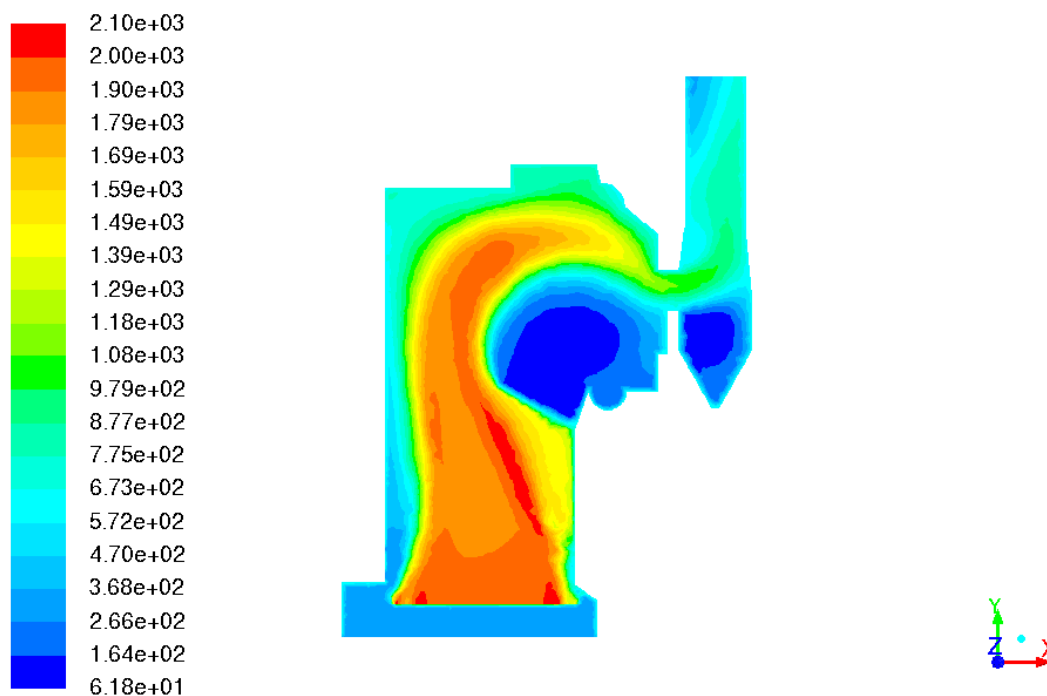


Figure 4.21. Temperature profile with the stack volume containing 33% of the negative energy source term

Even though the stack was now experiencing some circulation, there was still reduced circulation in the heat exchanger volume because of this source term splitting. Making the heat exchanger volume more realistic was more important than the appearance of a low temperature region in the bottom of the stack (which just catches particulates in the real boiler system), so another simulation was run with each section taking out half of the total energy. The temperature profile after 20,000 iterations is shown in Figure 4.22. After examining these results, it was clear that the circulation in the heat exchanger region was not improved significantly enough to conclude that spreading the heat absorption over a larger volume was an effective solution to the impossible temperature gradients and magnitudes. It seemed that in regions where the source term was present, extreme gradients and circulation regions were localized on the

center of the source term, while the area between the two circulations had more realistic temperatures.

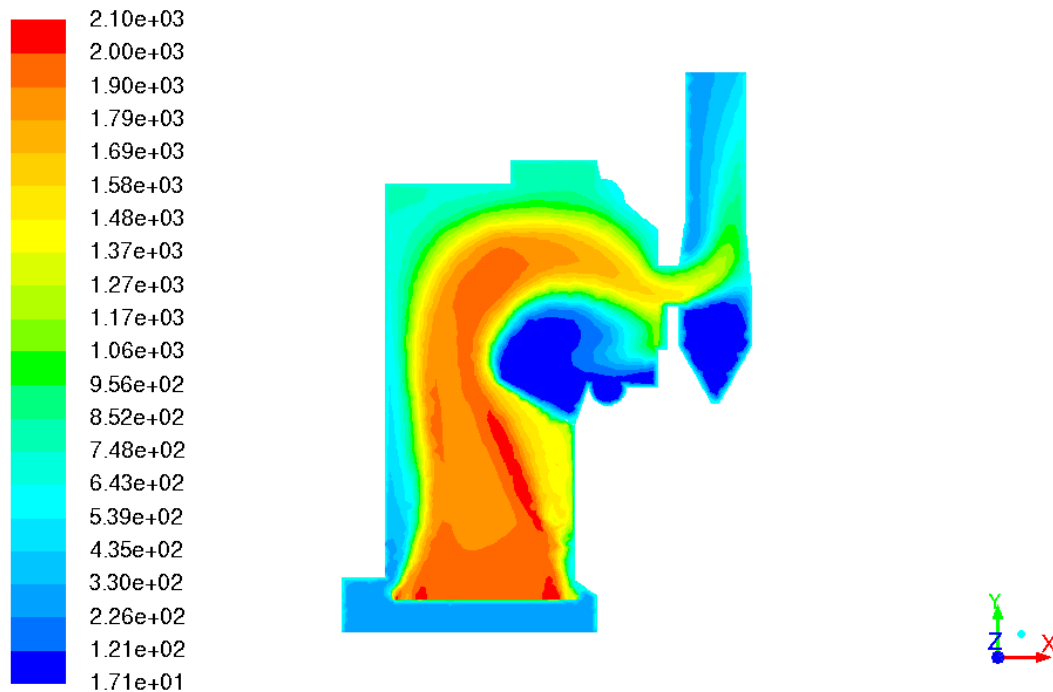


Figure 4.22. Temperature profile with the stack volume containing 50% of the negative energy source term

The next modification focused on the heat exchanger region only, splitting the volume into three horizontal sections. The reasoning behind this change was that most of the circulation was occurring in the region below the main flow path, and if the source term could be applied in the middle of the high temperature flow the gradients might not be as dramatic and the circulation below the flow path could be reduced. The large temperature gradients resulting from Fluent's calculations were assumed to be an effect of taking energy away from the flow in an area centered beneath it (the bottom of the heat

exchanger volume), which was initialized (along with the rest of the model) at a temperature of 1K. The sectioning of the heat exchanger volume allowed the energy to be taken out of the flow by a source that was in the center of the main flow path. Interestingly, after the temperature profile was obtained from the simulation results, it was observed that the circulation and temperature gradients were very similar to the original case where the entire heat exchanger volume contained the whole source term. Figures 4.23 and 4.24 show the geometric sectioning and the temperature profile after 10,000 iterations, respectively.

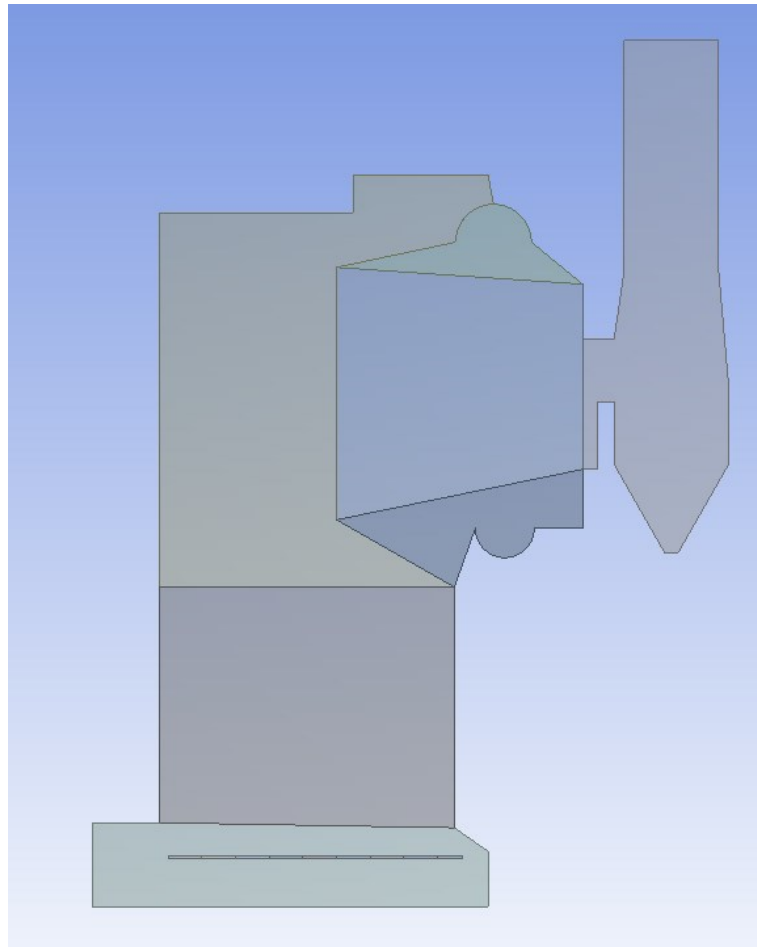


Figure 4.23. Modified heat exchanger volume geometry

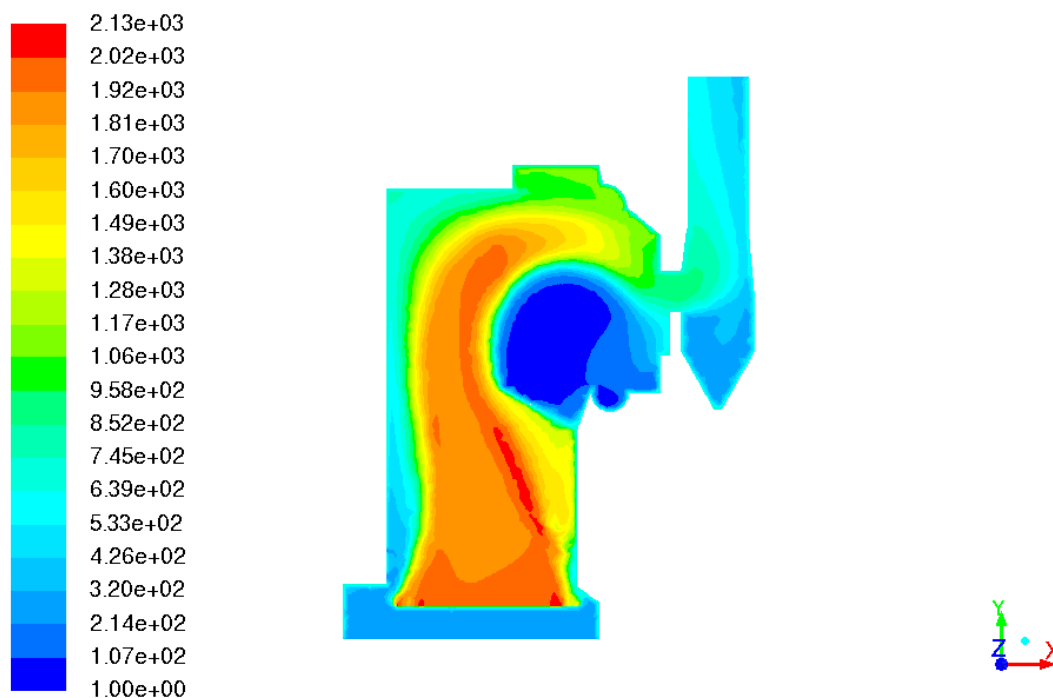


Figure 4.24. Temperature profile using modified heat exchanger volume geometry

After modifying the boundary conditions relating to the negative source term in the boiler model, it was evident that the method of using a sink to take energy from the flow was not the most effective way to obtain a realistic simulation of the boiler. Even though the energy sink model provided a quick simulation with low computational expense and a reasonable approximation of the flow path and maximum temperature regions inside the furnace, alternative heat exchanger approximations were needed to produce realistic results with the current model.

#### 4.4.2 Fluent Heat Exchanger Model

Fluent contains a feature used to approximate different types of heat exchangers, aptly named “Heat Exchanger Models.” Very little is known about these models, and



searches in journals, papers and articles return few instances where other researchers have used them. Fluent documentation has some limited information about the basic types of heat exchanger models that the software contains, as well as an introduction to the theory behind them. The general method used to simulate the water pipe heat exchanger in Unit 10 is the Macro Model. Figure 4.25 describes how a volumetric section representing a heat exchanger is divided into macros. Heat transfer between the heated gas in the furnace and the auxiliary fluid in the heat exchanger pipes is calculated using one of two models: the simple-effectiveness-model or the NTU-model. The simple-effectiveness model is able to allow phase change of the auxiliary fluid and is optimal when creating a network of heat exchangers using a Grouped Macro Model. The NTU-model, however, takes into account the specific heats of both the gas and the auxiliary fluid, can model heat transfer in both directions, is able to calculate reverse flow regions in the gas, and accounts for varying gas density. Both models can be used with either serial or parallel Fluent solvers.

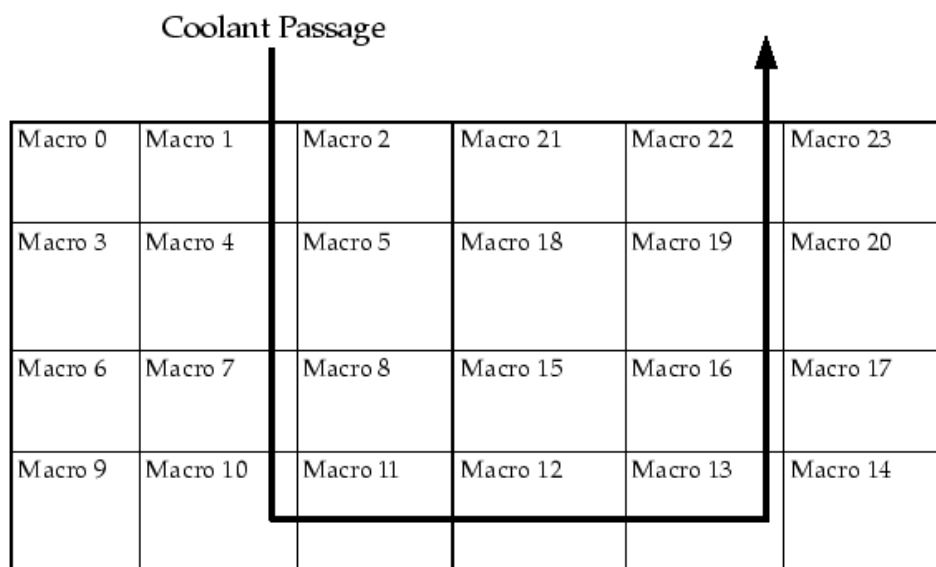


Figure 4.25. Macro sectioning used in Fluent heat exchanger models

## Theory

Necessary properties calculated with these heat exchanger models include streamwise pressure drop, core friction factor, heat transfer effectiveness, and heat rejection. For both models, streamwise pressure drop is given by Equation 16.

$$\Delta p = \frac{1}{2} f \rho_m U_{A_{min}}^2 \quad (16)$$

In the above equation,  $\rho_m$  is the mean gas density,  $U_{A_{min}}^2$  is the gas velocity at the minimum flow area, and  $f$  is the streamwise pressure loss coefficient, shown in Equation 17.

$$f = (K_c + 1 - \sigma^2) - (1 - \sigma^2 - K_e) \frac{v_e}{v_i} + 2 \left( \frac{v_e}{v_i} - 1 \right) + f_c \frac{A}{A_c} \frac{v_m}{v_i} \quad (17)$$

$K_c$  and  $K_e$  represent the entrance and exit loss coefficients, respectively,  $\sigma$  is the minimum flow to face area ratio,  $A$  and  $A_c$  are the gas-side surface area and minimum cross-sectional flow area,  $v_i$ ,  $v_e$ , and  $v_m$  are the inlet, exit and mean specific volumes, and  $f_c$  is the core friction factor, found with Equation 18.

$$f_c = a Re_{min}^b \quad (18)$$

In the above equation,  $a$  is the core friction coefficient,  $b$  is the core friction exponent, and  $Re_{min}$  is the Reynolds number for velocity at the minimum flow area.  $Re_{min}$  is found using the mean gas density and viscosity, core hydraulic diameter and gas velocity at the minimum flow area.

Within the simple-effectiveness-model, Equation 19 calculates the maximum heat transfer possible from the hot to cold fluid. The heat exchanger effectiveness,  $\epsilon$ , is the ratio of the actual heat transfer rate to the maximum rate. Using these ideas, the actual rate of heat transfer is found using Equation 20.

$$q_{max} = C_{min}(T_{in,hot} - T_{in,cold}) \quad (19)$$

$$q = \epsilon C_{min}(T_{in,hot} - T_{in,cold}) \quad (20)$$

The NTU-model utilizes the same equations for heat transfer that the simple-effectiveness-model does, but the exchanger effectiveness is more complicated as it incorporates the cell size and the specific heats for both fluids as shown in Equation 21.

$$\epsilon = 1 - \exp \left[ -\frac{1}{C_r} N_{tu}^{0.22} (1 - e^{-C_r N_{tu}^{0.78}}) \right] \quad (21)$$

In Equation 21,  $C_r$  is the ratio of the two fluid specific heats and  $N_{tu}$  represents the number of transfer units, which depends on the gas flow rate and the area of each macro. The gas inlet temperature present in the heat transfer equations is calculated using a mass average of the gas temperatures at the boundary of each macro, and as a result automatically takes into account any reversed flow.

The heat rejection for the simple-effectiveness-model is found on a cell-by-cell basis and summed up across each macro. It is then added to the energy equation for the gas flow as either a positive or negative source term, depending on the direction of heat transfer. Equation 22 gives cell-specific heat rejection.

$$q_{cell} = \epsilon (\dot{m} c_p)_g (T_{in,auxiliary\ fluid} - T_{cell}) \quad (22)$$

In the NTU-model, heat rejection is found for each macro using Equation 23. If needed, the cell heat rejection can be simply calculated by multiplying the macro heat rejection by the ratio of the cell volume to the macro volume. Both heat exchanger models determine total heat rejection using Equation 24.

$$q_{macro} = \epsilon C_{min}(T_{in,auxiliary\ fluid} - T_{in,gas}) \quad (23)$$

$$q_{total} = \sum_{All\ Macros} q_{macro} \quad (24)$$

After calculating heat transfer, the energy balance for each macro is solved to find the outlet auxiliary fluid temperature (based on the enthalpy). The resulting enthalpy and temperature of the auxiliary fluid leaving the macro are then used as inlet conditions for the solution of the next macro. The straightforward equations in the simple-effectiveness-model make it a suitable choice for a quick and fairly accurate approximation of multiple connected heat exchangers, containing many macros and cells. When simulating a single heat exchanger macro group, the NTU-model is the more logical option because of its ability to handle the varying properties and kinetics of the gas flow coming into each macro, resulting in a more accurate, albeit slower, solution than the simple-effectiveness-model could provide.

### Model Setup

Based on considerations related to the heat exchanger model theory, the NTU-model was used for the majority of the current Unit 10 boiler model simulations. Table 4.6 shows the relevant boundary conditions that were set for the first run using Fluent's heat exchanger models. The choices for the values and settings of the properties listed in the table are explained following the table.

Table 4.6. Various heat exchanger model parameter and settings

Model	NTU - Ungrouped Macro
Option	Fixed Inlet Temperature
Primary Fluid Temperature [K]	1.000
Primary fluid Flow Rate [kg/s]	25.00
Heat Transfer [W]	6.000E+08
Number of Passes	2
Number of Rows	5
Number of Columns	1
Auxiliary Fluid Specific Heat [J/kg-K]	4181
Auxiliary Fluid Flow Rate [kg/s]	19.53
Auxiliary Fluid Inlet Temperature [K]	486.4

The specific model type, “Ungrouped Macro”, means that the macro heat exchanger model in the selected region is not directly connected to any other heat exchanger volumes using macro divisions. In the simulation of Unit 10, there is only one fluid zone in which heat is transferred to the water pipes, so the “Ungrouped Macro” type is justified. The option “Fixed Inlet Temperature” means that the auxiliary fluid (water, in this case) coming into the heat exchanger pipes is always at the same temperature. This makes sense for this simulation, as the water in the real system would always come into the boiler at a temperature specified by the operator. The value for this property in the table above comes directly from measurements taken by the UI power plant. The boundary condition for the primary fluid temperature relates to the temperature of the combusted gas flow coming into the heat exchanger volume section. This value depends on the results of the combustion and turbulence modeling in the furnace section of the model and was therefore set to a minimum initial guess. The auxiliary fluid flow rate was obtained using data received from the power plant. By calculating the flow rate of the

superheated gas traveling from the upper furnace volume to the heat exchanger volume in the previous simulations covered in this work, the primary fluid flow rate coming into the exchanger was able to be estimated. The total heat transfer from the gas to the water was fixed by the amount of energy needed to produce a 100% steam load in the Unit 10 boiler. Using the heat exchanger section's total volume, a simple calculation converting the negative energy source term from Watts per unit volume to Watts was done to obtain the total heat transfer value given in the table. The number of passes, rows, and columns are referencing the macro divisions (seen previously in Figure 4.25) and were left at the default values set by Fluent. Since little was known about Fluent's heat exchanger models at the time of the first simulation run, default values for these conditions were kept, and subsequent simulations would be used to determine the effect each condition had on the boiler model. The remaining value in the table simply gives the specific heat of the water used as the auxiliary fluid in the heat exchanger pipes, and was found in a fluid mechanics textbook (White 2011).

### Simulations with the Fluent Heat Exchanger Models

Using the parameters outlined in the previous section, the first analysis of the boiler was run using Fluent's NTU heat exchanger model. From Figure 4.26, it is evident that this model yielded immediate improvement in the circulation and temperature gradients present in the heat exchanger volume. Large regions with unrealistically low temperatures (1 to 100K) are completely eliminated and the flow circulates much less intensely below the main flow path. The stack region has almost constant gas temperatures and only small gradients remain at the wall boundaries. This is a strong indicator of more realistic results, as the gas in the real boiler will come out of the economizer section (between the heat exchanger and the stack) at a lower, more uniform

temperature. Previous simulations showed poor temperature mixing in the stack, including regions of high temperature gradients and low temperature magnitudes. The velocity vectors can be seen in Figure 4.27. The main flow stream can still be clearly identified, and the path is a logical one for the boiler geometry used in the simulation.

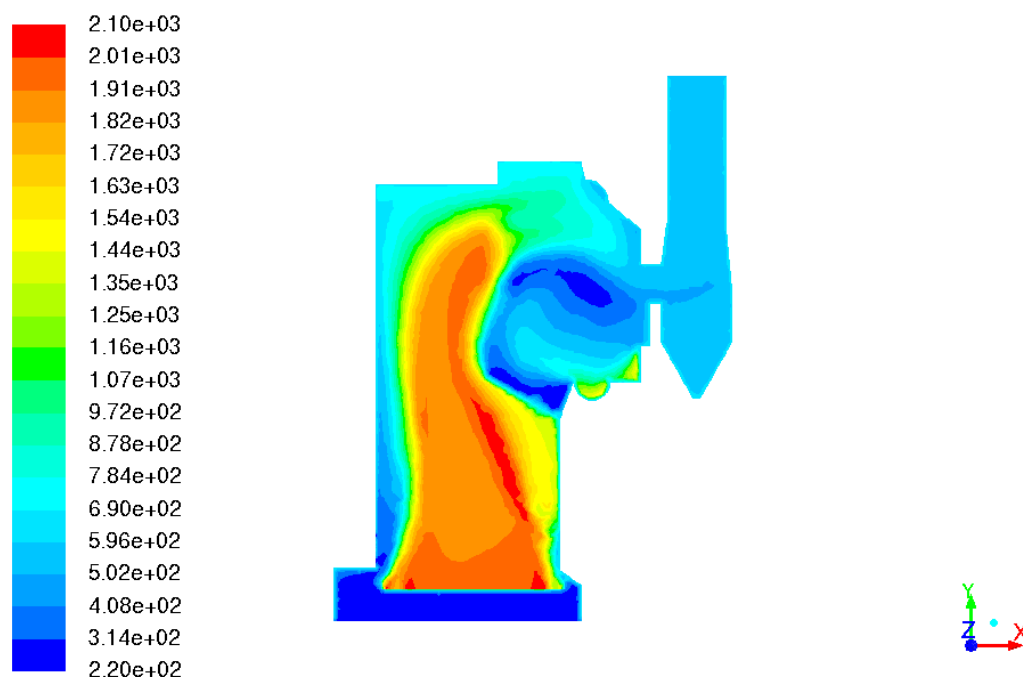


Figure 4.26. Temperature profile from initial Fluent heat exchanger model simulation

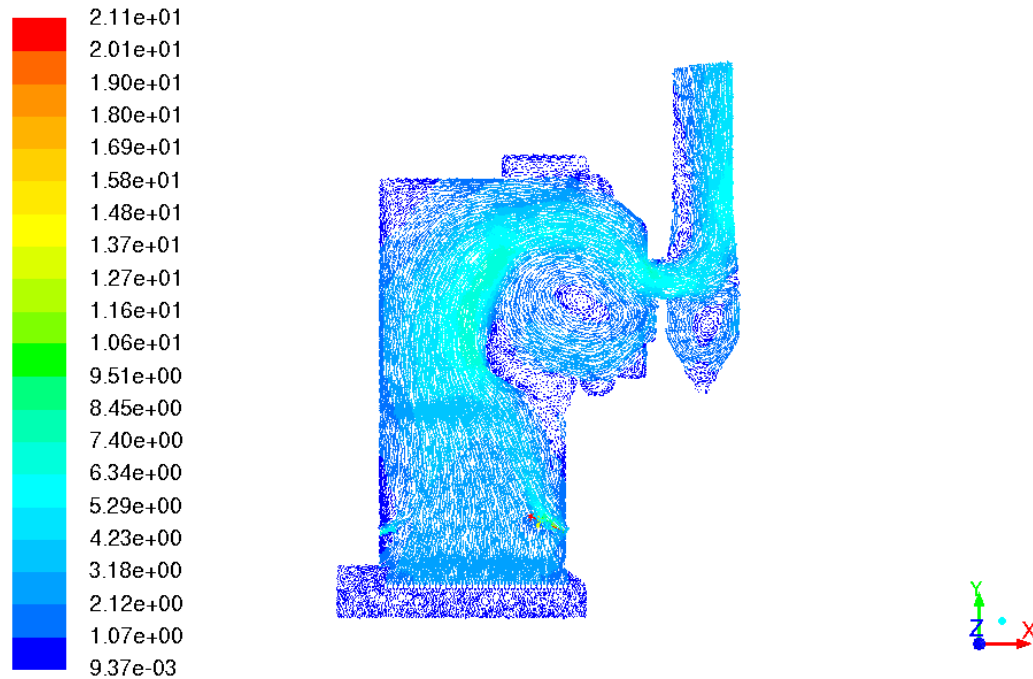


Figure 4.27. Velocity vector profile from initial Fluent heat exchanger model simulation

The other heat exchanger model, the simple-effectiveness-model, was used in the next simulation. All other conditions were kept the same and the model analysis was run again, yielding the temperature profile shown in Figure 4.28 after 10,000 iterations. Surprisingly, it was similar to the results from the original simulations where the source term took the place of the heat exchanger model. A large amount of circulation is again seen in the heat exchanger volume and there is some in the bottom of the stack. The maximum temperature is higher than in the simulation run with the NTU-model, and there are unrealistically low temperatures present in the boiler again. The assumption made in the heat exchanger model theory section of this chapter, that the simple-effectiveness-model is more useful for large amounts of macros and connected heat exchanger groups while the NTU-model is more accurate for small heat exchanger macro



groups, is partially verified by the results of this simulation. Further verification could come from a comparison between the simple-effectiveness-model and NTU-model for connected heat exchanger groups, which is out of the scope of this work.

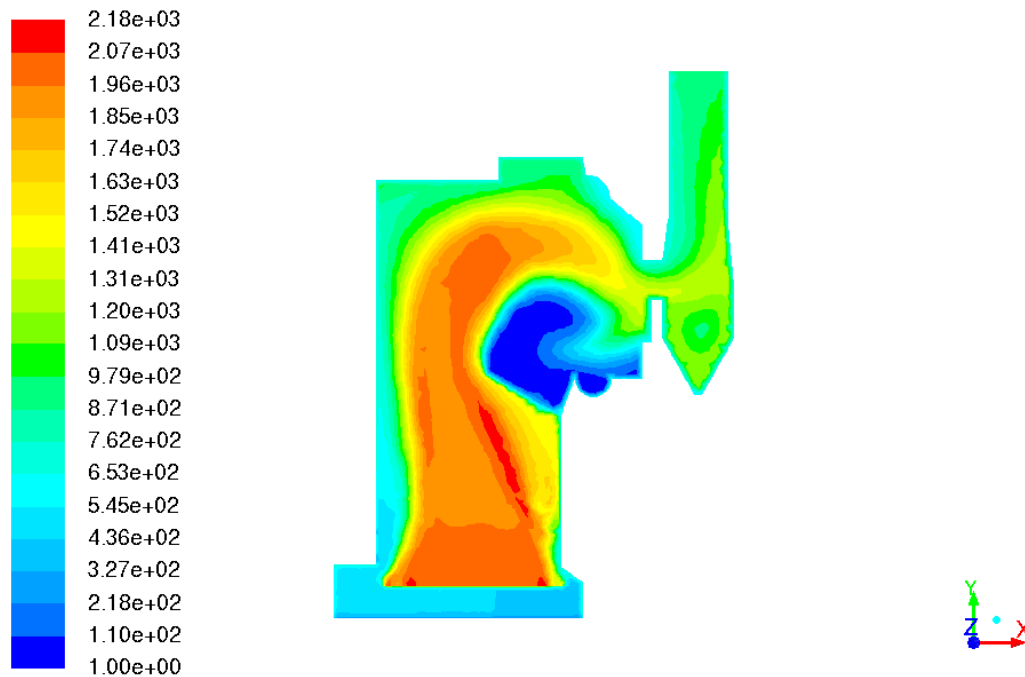


Figure 4.28. Temperature profile using simple effectiveness model

Using the NTU-model for the rest of the simulations, more tests were done to study Fluent's heat exchanger modeling capabilities. The first was comparing the settings "Fixed Inlet Temperature" and "Fixed Heat Rejection". The initial analysis, discussed above, used the "Fixed Inlet Temperature" boundary condition, so a case was run with "Fixed Heat Rejection" instead. The temperature profile (Figure 4.29) showed a logical flow path and temperature distribution, but the magnitudes were much larger, including very high temperatures in the heat exchanger (1200-1300K) and coming out of the stack

(1600-1900K). The temperature of the gas coming out of the stack is unreasonable for a real system, and it seems like the heat exchanger model did not remove enough energy from the flow, which started out at a very high temperature above the grate. Since the boundary condition being tested was “Fixed Heat Rejection”, it was assumed that the model probably lowered the temperature of the water in the heat exchanger pipes to incredibly low values in order to take out the specified amount of heat. This was a large assumption based on limited knowledge about the heat exchanger models, but the decision was made to continue simulations using the “Fixed Inlet Temperature” boundary condition instead. The inlet temperature of the water in the heat exchanger is set by the power plant, so other settings in the heat exchanger model were changed in order to improve the results.

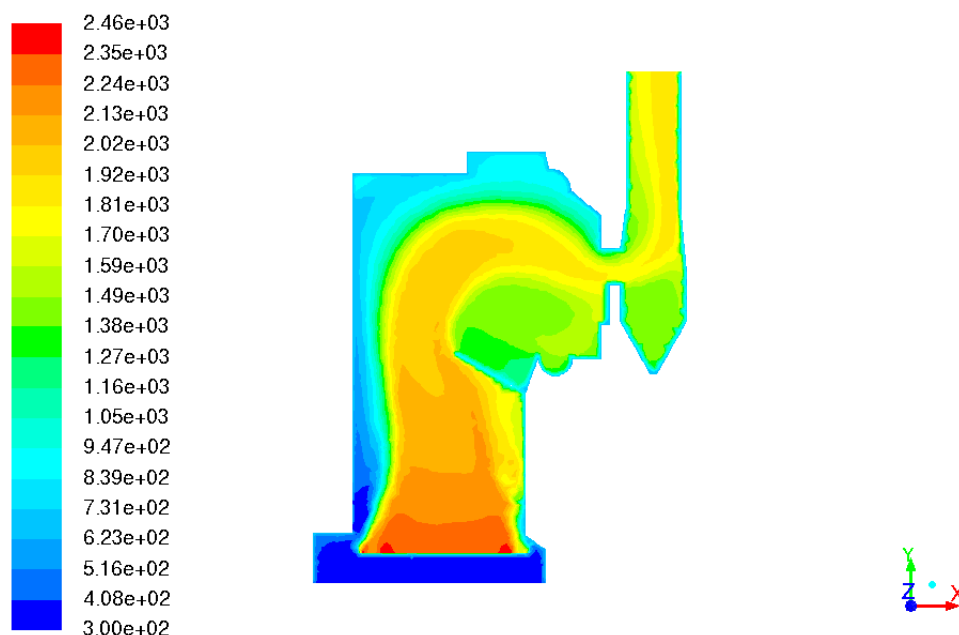


Figure 4.29. Temperature profile using Fixed Heat Rejection

The next simulations were done to examine the effect of changing the macros in different ways. First, the number of passes the water makes through the heat exchanger volume as it goes through the simulated “pipes” was varied to see if a trend emerged. The initial simulation used two passes, so the temperature profiles from cases using three, four, five and six passes are shown in Figures 4.30 to 4.33. It is harder to tell what the main flow path is just from examining these temperature distributions, so the velocity vectors for each case are displayed in Figures 4.34 to 4.37. Two things are happening as the heat exchanger increases from three to six passes: the maximum temperature in the boiler decreases and the heat exchanger volume becomes more uniform in temperature. Both of these trends make sense; as the effective number of heat exchanger pipes increases, heat is removed more efficiently from the boiler, lowering the overall temperature, and since the volume is fixed, the passes get closer together, thereby removing energy from the region with better resolution. A side effect of adding more passes was that the iteration steps converged more slowly, leading to some “rough” areas in the temperature profile, which are most evident in the six pass case. For the purposes of further simulations, the five pass case was chosen as the base model. It has a lower stack temperature than the four pass simulation, a more symmetrical heat exchanger temperature profile, and shows a distinct temperature difference between the stack and main flow path, more closely resembling the real system where the flow loses most of its energy in the exchanger portion of the boiler.

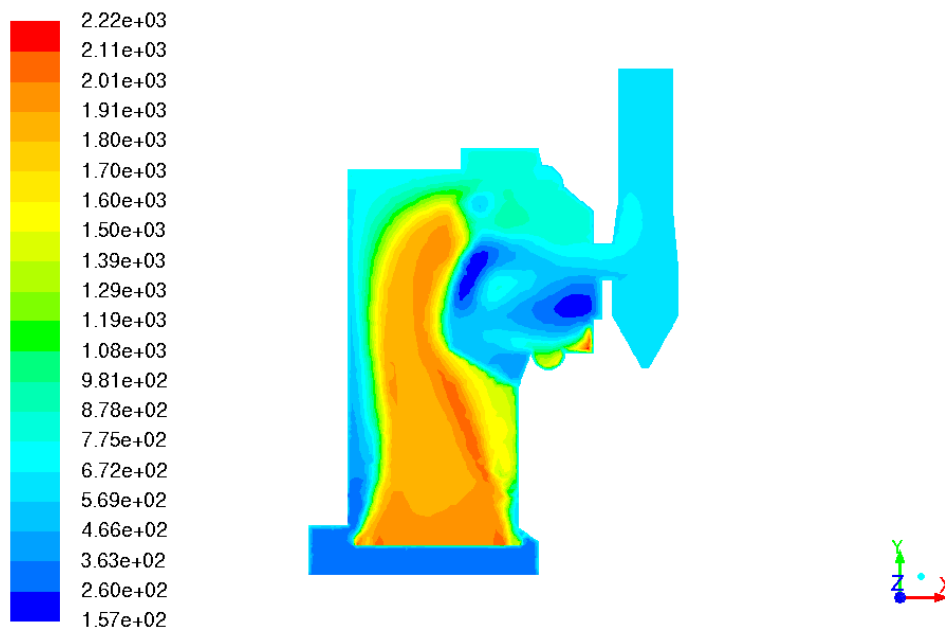


Figure 4.30. Temperature profile using NTU model with three passes

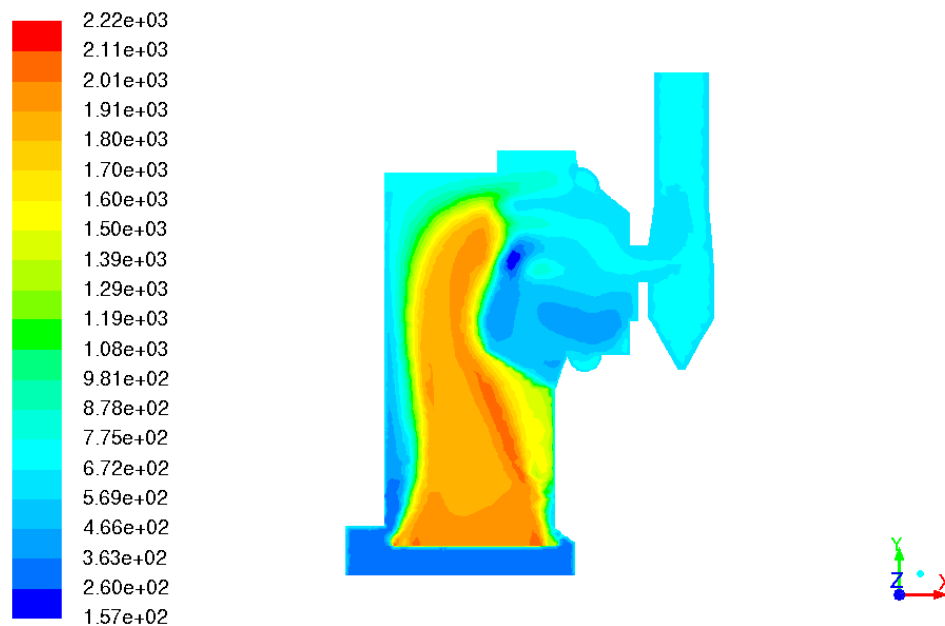


Figure 4.31. Temperature profile using NTU model with four passes

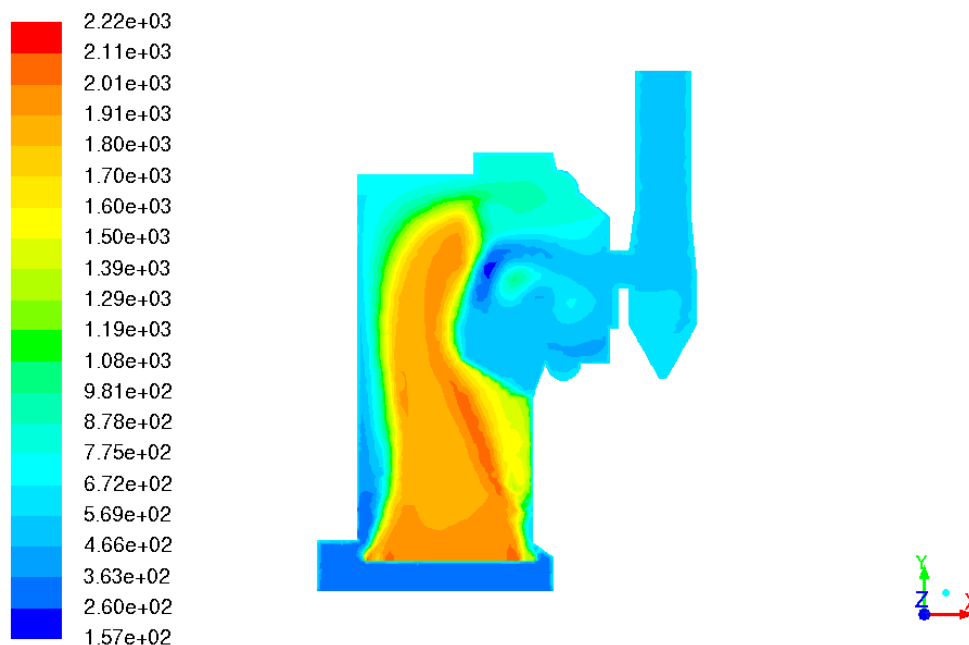


Figure 4.32. Temperature profile using NTU model with five passes

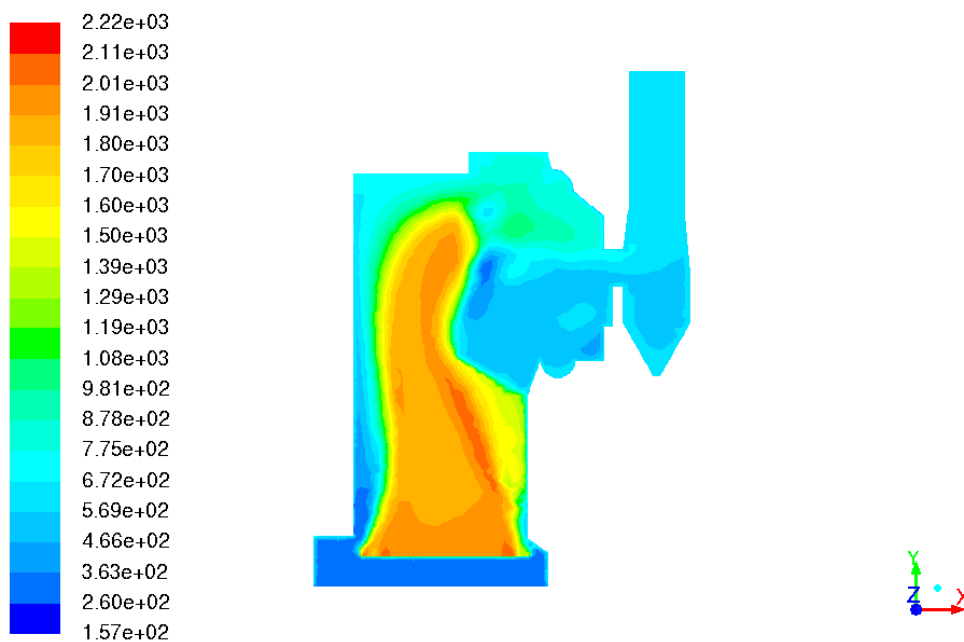


Figure 4.33. Temperature profile using NTU model with six passes

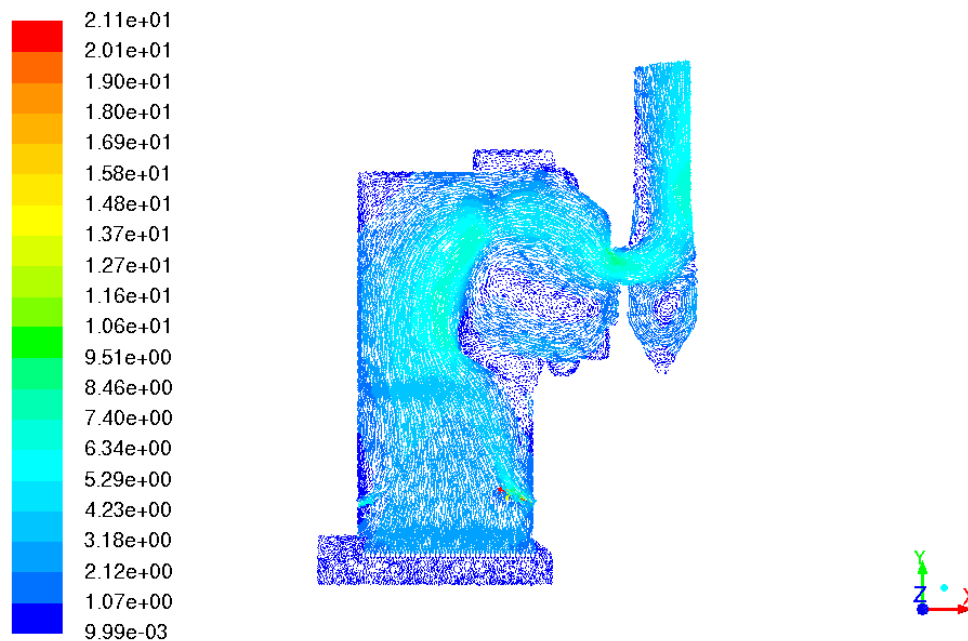


Figure 4.34. Velocity vector profile using NTU model with three passes

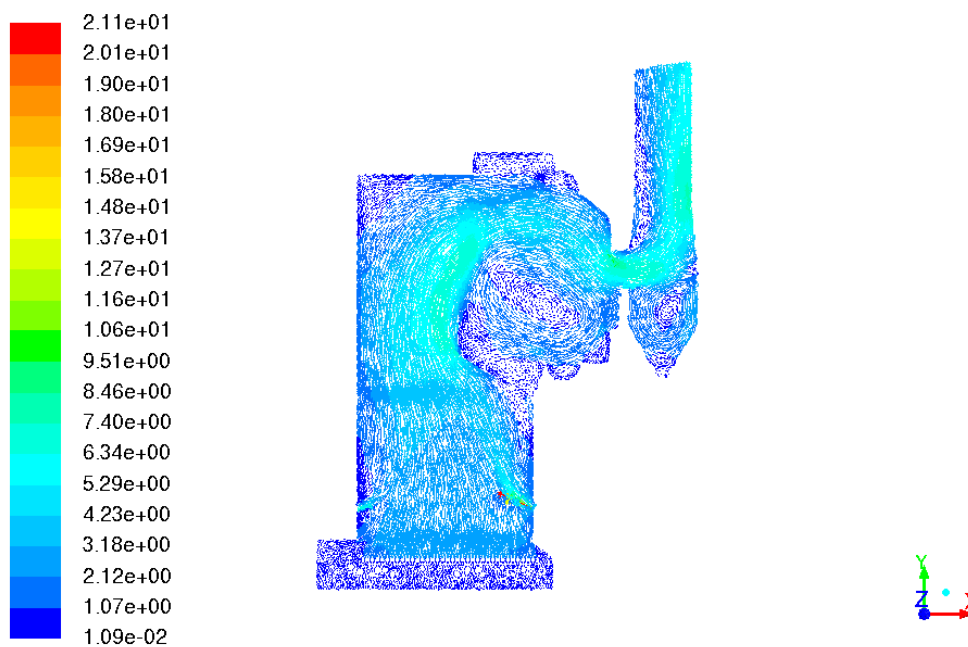


Figure 4.35. Velocity vector profile using NTU model with four passes

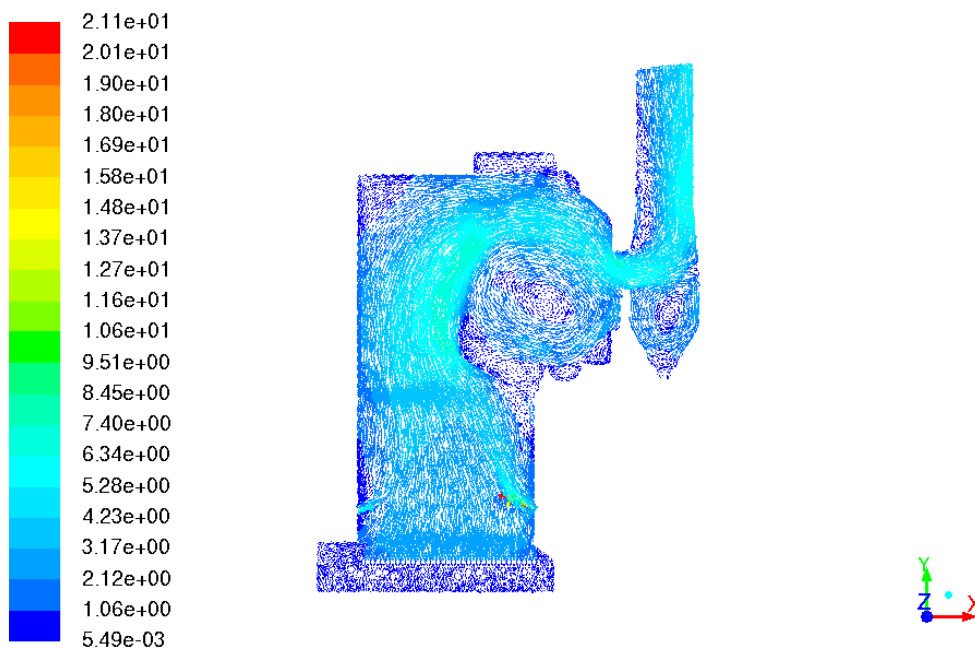


Figure 4.36. Velocity vector profile using NTU model with five passes

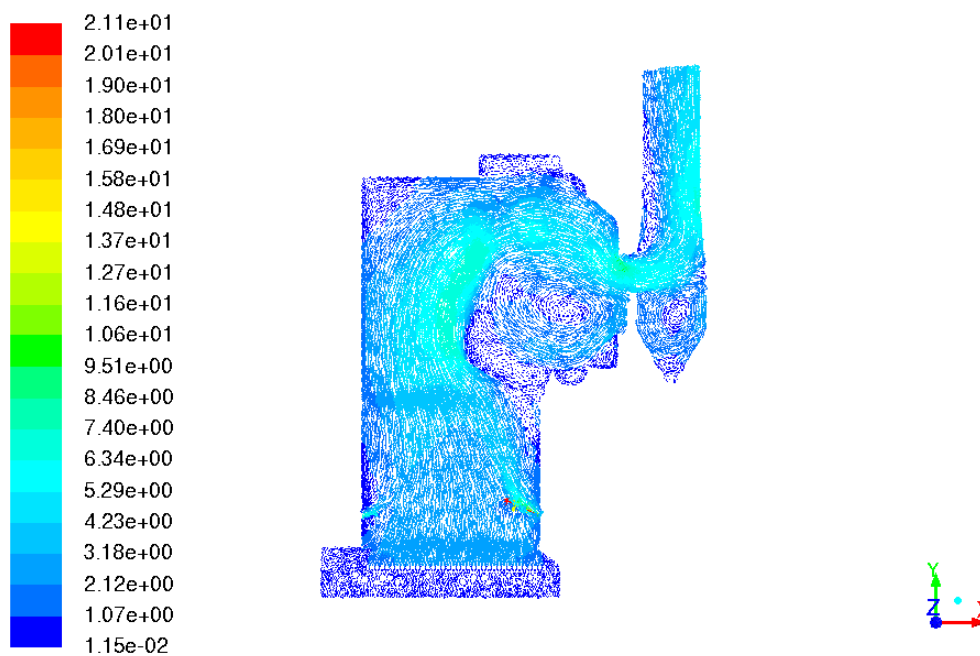


Figure 4.37. Velocity vector profile using NTU model with six passes

To further increase the resolution of the heat exchanger, the number of rows was modified. The initial heat exchanger model analysis had five rows, so the temperature profiles for six, 10 and 15 rows are shown in Figures 4.38 to 4.40. Adding rows significantly increased the uniformity of the temperature distribution in the heat exchanger volume because of the resulting higher macro resolution in the NTU-model. As the number of rows grew, however, the convergence speed decreased, which makes sense because of the increased resolution. The case with 15 rows did not converge as well as the six or the 10 row cases, so the latter cases were used for further simulations.

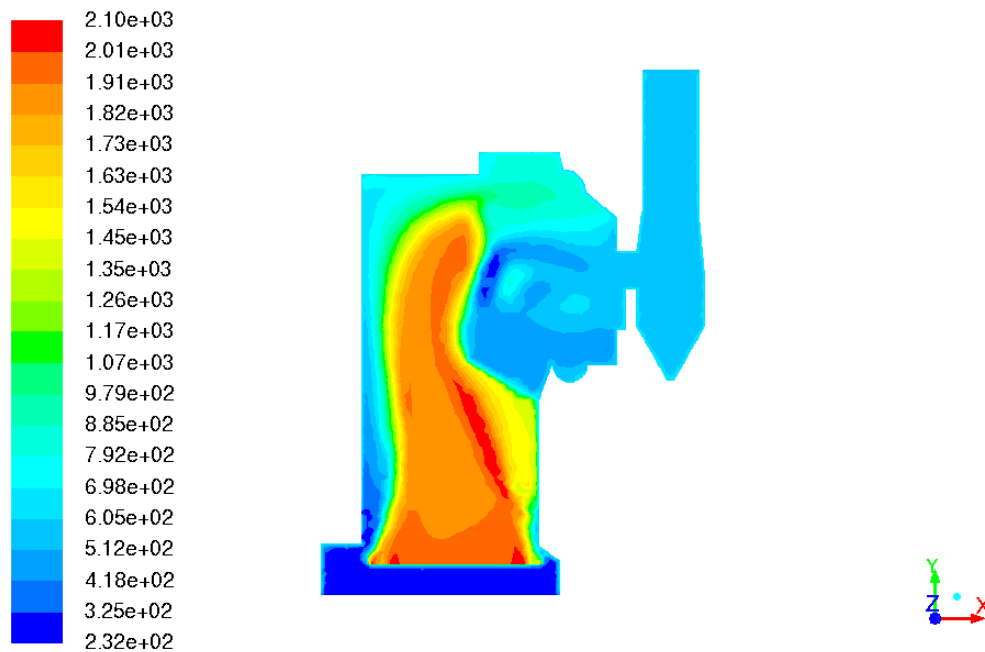


Figure 4.38. Temperature profile using NTU model with five passes and six rows



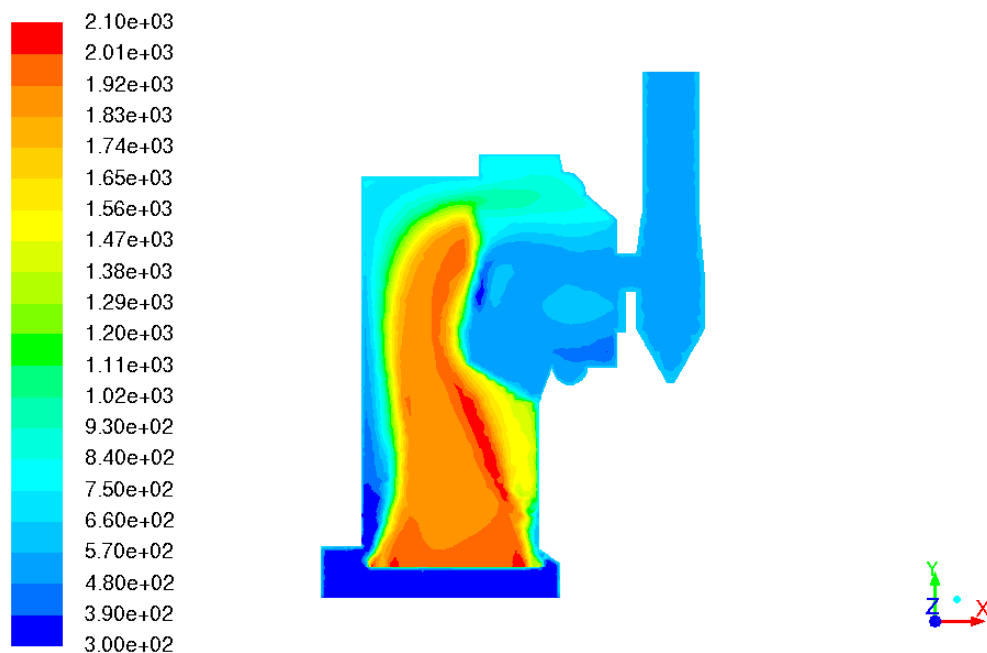


Figure 4.39. Temperature profile using NTU model with five passes and 10 rows

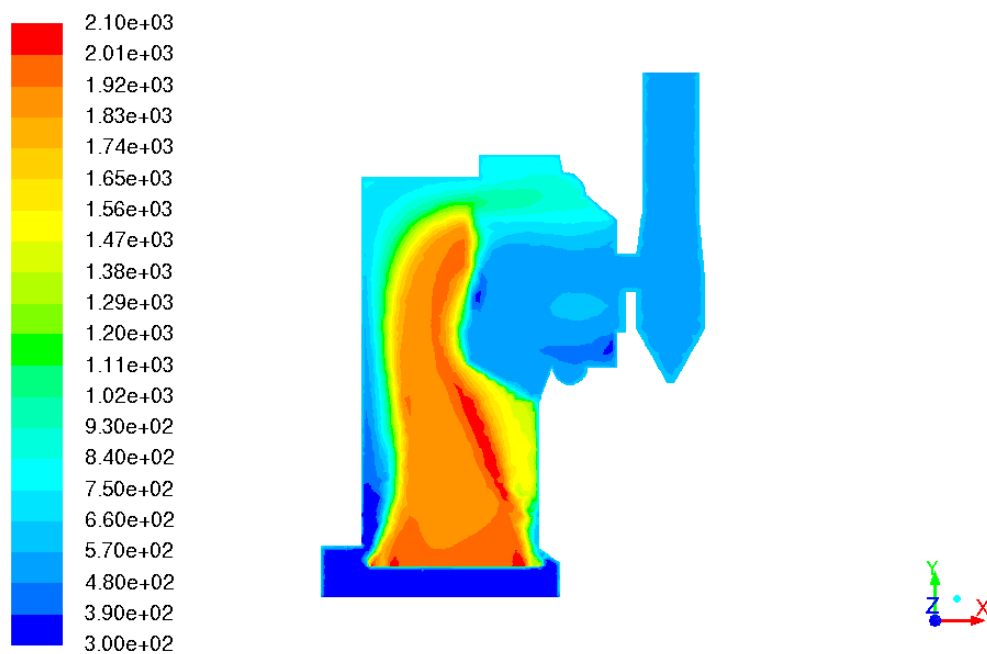


Figure 4.40. Temperature profile using NTU model with five passes and 15 rows

Final simulations done with the heat exchanger model consisted of combining the modified secondary inlet velocity cases with the two best NTU-model cases. The goal of these combined cases was to see if the circulation and high temperature gradients could be eliminated along with the reduction of high temperature regions in the middle furnace region. Figure 4.41 shows the temperature profile resulting from the combination of the NTU-model with fixed inlet temperature, five passes and six rows, and a small secondary inlet air velocity of 10 m/s. The temperature profile resulting from the combination of the NTU-model with fixed inlet temperature, five passes and 10 rows, and a small secondary inlet air velocity of 10 m/s is displayed in Figure 4.42. After examination of both figures, it seems that the temperature profile is a simple superposition between the profile from the modified velocity case and the one from the NTU-model case. This is a useful observation to make, since further testing of cases with combinations of different modifications can be predicted without necessarily needing to run full simulations.

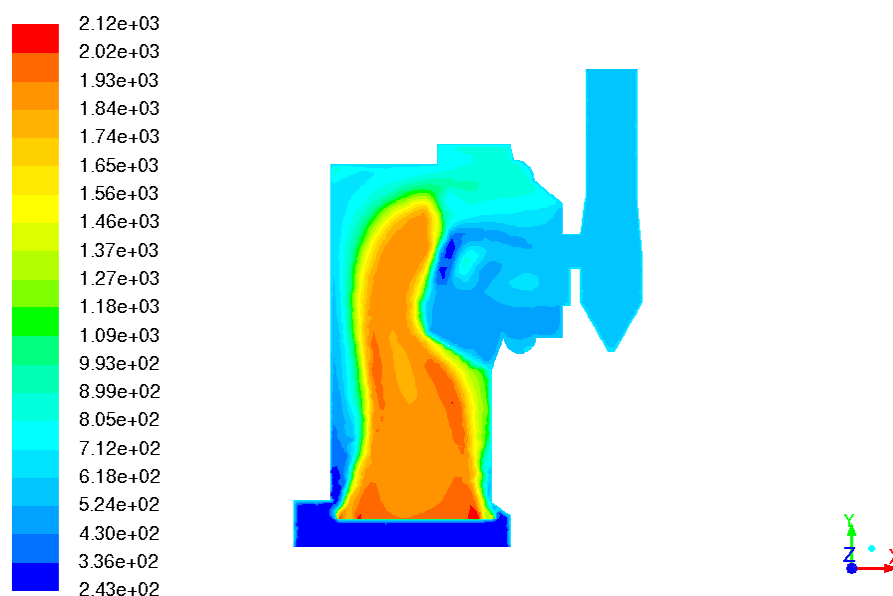


Figure 4.41. Temperature profile using NTU model with 6 rows in combination with 10 m/s small secondary inlet velocity

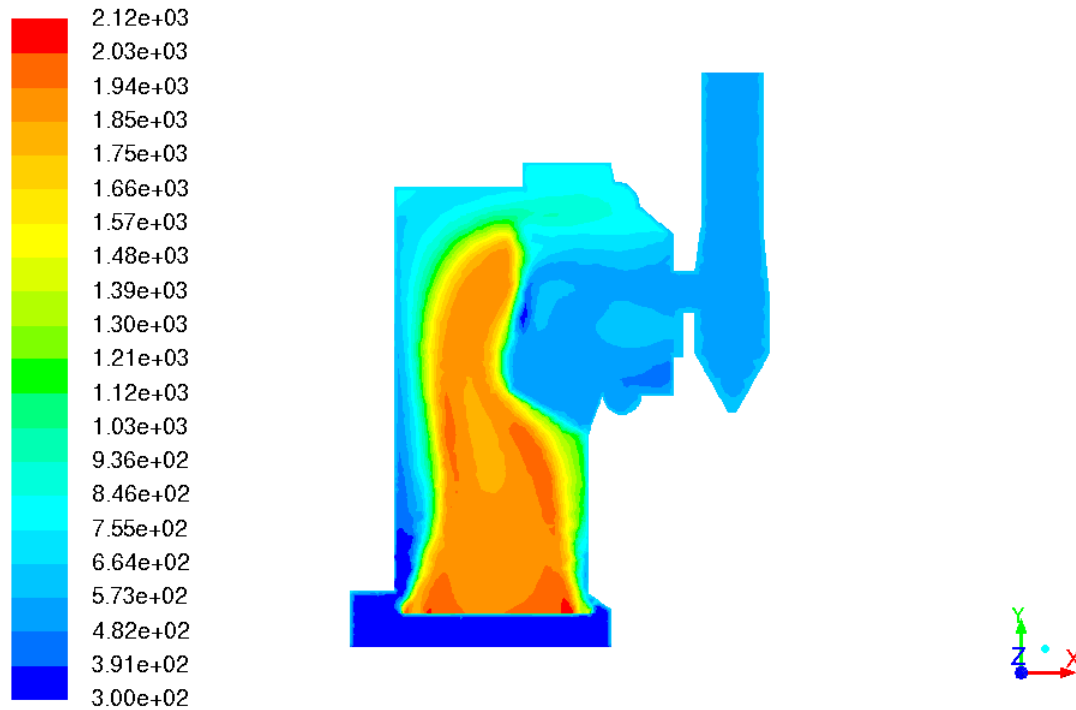


Figure 4.42. Temperature profile using NTU model with 10 rows in combination with 10 m/s small secondary inlet velocity

From the results presented above, it is clear that the Fluent heat exchanger models are effective at modeling the heat transfer and rejection from a heated gas flow in a combustion simulation. In order to achieve similar results using negative source terms (energy sink boundary conditions), the heat exchanger would have to be discretized into many volumes, and energy source terms would have to be applied in each. The heat exchanger models, however, use an energy balance for each “macro” in the group, thus increasing the resolution in a quicker and more accurate way. A significant effect resulting from the use of the heat exchanger model was that the conservation equations followed a monotonic convergence as the iteration steps progressed. This was a definite improvement over the rough oscillatory convergence during simulations of the earlier

models using negative energy source terms. As an example, Table 4.7 lists the final convergence values of the continuity, momentum, and energy equations for a case using a negative source term over the whole exchanger volume (20,000 iterations) versus the initial NTU-model simulation case (10,000 iterations). The case using Fluent's heat exchanger model converged much faster than the case using the energy sink and was more accurate to two orders of magnitude.

Table 4.7. Comparison of final convergence values for key equations

	Source Term Case	Heat Exchanger Case
Continuity	1.17E-02	6.99E-04
X-Velocity	6.13E-03	2.95E-05
Y-Velocity	4.89E-03	2.67E-05
Z-Velocity	4.26E-03	1.72E-05
Energy	1.54E-03	1.51E-05

## CHAPTER 5: CONCLUSIONS

### 5.1 Conclusions

In this work, updated models based on a previously existing Unit 10 stoker boiler model were created and used to run simulations testing various boundary conditions, flow models, and energy balance methods. Boundary condition modifications included modifying the geometry and mesh grid, matching wall temperatures to actual operating conditions, updating the coal proximate and ultimate analyses, and varying secondary air inlet velocities.

The realizable  $k - \varepsilon$  turbulence model and the P1 radiation model, also used in previous simulations by Zhang, were determined to be the most accurate models for this specific boiler model. It was found that lowering air speeds at the smaller secondary inlets decreased localized zones of high temperature and resulted in a more uniform temperature profile in the boiler furnace. However, as the air velocities decreased, the values became further from the operating conditions of the boiler, a fact which detracted from the goal of developing a realistic model that could be used to accurately simulate conditions in a real system.

After multiple different mesh grids and geometries, it was determined that the existing geometry was the most realistic, and the existing mesh grid (with slight coarsening) resulted in relatively fast simulations, with negligible decreases in the accuracy of the flow path or temperature profile in the boiler.

Different energy balance methods were implemented in order to reduce the circulation and high temperature gradients present in the heat exchanger volume section of the boiler model. These methods included splitting the negative energy source term (representing the heat loss to the water pipes in the real boiler's heat exchanger) across the heat exchanger volume itself and applying different fractions of the source term

between the heat exchanger and stack volumes. Results from these modifications showed continued circulation and impossibly low temperatures (i.e. 1-100 K) in the heat exchanger and stack regions, and these poor results led to the research, testing, and implementation of Fluent's built-in heat exchanger models.

Fluent contains two major heat exchanger models: the simple-effectiveness-model and the NTU-model. Both discretize the selected volume into "macros", wherein an energy balance is applied and heat fluxes are calculated to determine the heat transfer from the heated gas flow to the auxiliary fluid in the heat exchanger pipes (which is water, in the case of Unit 10). These calculations give temperature data at the boundary of each macro, resulting in an approximate temperature profile over the specified region. The simple-effectiveness-model is more suited for multiple connected heat exchanger macro groups, while the NTU-model is accurate for a single heat exchanger section with varying amounts of macros. Implementation of the NTU-model showed immediate improvement in the circulation and temperature gradients within the heat exchanger volume. Though some circulation is still present, as in a real system, there are very few unrealistic temperature regions remaining in the entire boiler model.

The number of macros in the heat exchanger region was increased in two different ways: by increasing the number of passes the water in the pipes made through the volume and by increasing the number of rows each pass went through. Both of these methods effectively increased the resolution of the volume by decreasing the respective size of each macro as more were added, and when they were combined the temperature profile accuracy improved. A negative effect resulting from adding more macros was that the simulation time increased because equations solved by Fluent did not converge as quickly and the solution ended up behaving asymptotically before getting close to convergence limits set in the model. The NTU-model simulation cases with the most accurate results were combined with the lower secondary inlet velocity cases (discussed above), and the results showed a superposition of the respective temperature profiles individually

displayed by each of the methods: the circulation and temperature gradients were minimized in the heat exchanger volume and the localized high temperature zones above the bed were decreased in magnitude and size.

## 5.2 Future Work

Using the promising results from the Fluent heat exchanger models, different cases computing  $\text{NO}_x$  emissions can be run to compare with measured values and predict emission levels at different coal loading conditions on the boiler. In addition, various biomasses (lignin, wood chips, etc.) or natural gas can be combined with the coal in the model, and simulations can be run to determine the effect these renewable fuels have on the emissions of a stoker boiler.

In order to utilize the models presented in this work with other types of boilers, the bed model should be modified and tested using methods discussed in Chapters 2 and 3. Then the boundary conditions, flow models, and heat exchanger models used in this work can be applied to other systems to study various combustion conditions, including basic coal combustion, biomass combustion, and  $\text{NO}_x$  reduction methods.

## REFERENCES

- N. W. Ford, M.J. Cooke, and P.W. Sage. Modelling of fixed bed combustion. *Fuel Processing Technology*, 36: 55-64, 1993.
- K. Goerner and T. Klasen. Modeling, simulation and validation of the solid biomass combustion in different plants. *Progress in computational fluid dynamics*, 6(4-5):225-234, 2006.
- S. K. Kær. Straw combustion on slow-moving grates—a comparison of model predictions with experimental data. *Biomass and Bioenergy*, 28(3):307-320, 2005.
- S. E. Kim, D. Choudhury, and B. Patel. Computations of Complex Turbulent Flows Using the Commercial Code **FLUENT**. In *Proceedings of the ICASE/LaRC/AFOSR Symposium on Modeling Complex Turbulent Flows*, Hampton, Virginia, 1997.
- R. P. van der Lans, L.T. Pedersen, A. Jensen, P. Glarborg, and K. Dam-Johansen. Modeling and experiments of straw combustion in a grate furnace. *Biomass and Bioenergy*, 19(3):199-208, 2000.
- B. E. Launder and D. B. Spalding. *Lectures in Mathematical Models of Turbulence*. Academic Press, London, England, 1972.
- C. Lin, L. Rosendahl, and T. J. Condra. Further study of the gas temperature deviation in large-scale tangentially coal-fired boilers. *Fuel*, 82: 1127-1137, 2003.
- M. Miltner, A. Miltner, M. Harasek, and A. Friedl. Process simulation and CFD calculations for the development of an innovative bale biomass-fired combustion chamber. *Applied Thermal Engineering*, 27: 1138-1143, 2007.
- Patankar SV. Numerical heat transfer and fluid flow. Hemisphere 1980.
- R. Sharler, M. Forstner, M. Braun, T. Brunner, and I. Obernberger. Advanced CFD Analysis of Large Fixed Bed Biomass Boilers with Special Focus on the Convective Section. In *2<sup>nd</sup> World Conference and Exhibition on Biomass for Energy, Industry and Climate Protection*, Rome, Italy, 2004.
- T. H. Shih, W. W. Liou, A. Shabbir, Z. Yang, and J. Zhu. A New  $k$ - $\epsilon$  Eddy-Viscosity Model for High Reynolds Number Turbulent Flows - Model Development and Validation. *Computers Fluids*, 24(3):227-238, 1995.
- P. R. Solomon, D. G. Hambleton, R.M. Carangelo, M. A. Serio, and G. V. Deshpande. General Model of Coal Devolatilization. *Energy & Fuels*, 2: 405-422, 1988
- Steam: Its Generation And Use*, 38th Edition, Babcock and Wilcox, New York, 1975.
- D. Wei and W. Blasiak. CFD modeling of ecotube system in coal and waste grate combustion. *Energy Conversion and Management*, 42(15-17):1887-1896, 2001.
- F. M. White (2011). *Fluid Mechanics* (7<sup>th</sup> ed.). New York, NY: McGraw-Hill.



- Y. B. Yang, R. Newman, V. N. Sharifi, J. Swithenbank, and J. Ariss. Mathematical modelling of straw combustion in a 38 MWe power plant furnace and effect of operating conditions. *Fuel*, 86(1-2):129-142, 2007.
- Xinhui Zhang. "Numerical modeling of biomass combustion in a stoker boiler." dissertation, University of Iowa, 2011. <http://ir.uiowa.edu/etd/3023>.
- Xinhui Zhang, Mohsen Ghamari, Albert Ratner. Numerical modeling of co-firing a light density biomass (*Avena sativa*) hulls, and chunk coal in fluidized bed boiler. *Biomass and Bioenergy*, 56: 239-246, 2013.
- H. Zhou, A.D. Jensen, P. Glarborg, P.A. Jensen, and A. Kavaliauskas. Numerical modeling of straw combustion in a fixed bed. *Fuel*, 84(4):389-403, 2005.